

Soft EPMs:
Design and Fabrication of Soft Composite Materials for
Soft Electro-magnetic Actuators

by

Billy Koech

S.B. Degree Candidate in Electrical Engineering
Faculty Advisors – Professor Radhika Nagpal
And
Dr. Bahar Haghight

*A senior design project submitted in partial fulfillment of the
requirements for the degree of Bachelor of Science at Harvard University*

Harvard University
School of Engineering and Applied Sciences
Cambridge, MA
April 2020

Table of Contents

<i>I. Introduction</i>	5
A. Problem Statement.....	5
B. Stakeholders.....	5
<i>II. Background Research</i>	6
A. Characterization of magnetic materials.....	6
B. Magnetic Material Types.....	6
C. Electromagnets.....	8
D. Electropermanent magnets.....	8
E. Motivation for using EPMs.....	9
<i>III. Design Goals and Technical Specifications</i>	9
A. Goals.....	9
B. Device Size/Scale.....	10
C. Holding Force.....	10
D. Soft Iron End Permeability.....	10
E. Soft Iron End Compliance.....	10
F. Hard Permanent Magnet Coercivity.....	11
G. Hard Permanent Magnet Compliance.....	11
H. Semi-hard Permanent Magnet Coercivity.....	11
I. Semi-hard Permanent Magnet Compliance.....	11
J. Coil Conductivity.....	11
K. Coil Magnetic field strength (H).....	12
L. Coil transient current limit.....	12
<i>IV. Technical Design Approach</i>	12
A. Latch Flexibility alternatives:.....	12
B. Soft Iron End Design: Permeability-Flexibility trade off.....	13
C. Soft coil Design: Current-Turns trade off.....	14
D. Flexible permanent magnet design: Force flexibility trade off.....	15
<i>V. Building/Prototyping</i>	17
A. Soft Iron End Prototype.....	17
B. Soft Coil prototype.....	19
C. Magnetic core prototype.....	21
<i>VI. Evaluation/ Verification</i>	22
A. Soft Iron Ends Measurements and Verification.....	22

B.	Soft Coil Measurements and Verification.....	24
C.	Magnetic Core Measurement and Verification.....	26
D.	Assembled Device Measurement and Verificaiton.....	26
VII.	<i>Budget</i>	27
VIII.	<i>Conclusion and Future work</i>	27
A.	Summary of Achieved Technical Specifications	27
B.	Discussion	27
C.	Future Work	28
IX.	<i>Acknowledgment</i>	28
X.	<i>References</i>	28
XI.	<i>APPENDICES</i>	29

Table of figures

Fig. 1.	Stakeholder map. SSR: Self Organizing Systems Research	6
Fig. 2.	System diagram showing the where soft Electropermanent magnet (EPM) actuators reside in a larger system.	6
Fig. 3.	Example B-H graph of diamagnetic and paramagnetic materials.....	7
Source:	Adapted from [6]	7
Fig. 4.	Example B-H graph of a ferromagnetic materials.	7
Source:	Adapted from [6]	7
Fig. 5.	Example B-H graph of soft and hard ferromagnetic materials.	7
Source:	Adapted from [6]	7
Fig. 6.	Rigid version of an Electropermanent Magnet	8
Source:	Adapted from [4]	8
Fig. 7.	Principle of operation of an EPM with just a semi-hard magnet, a hard magnet and a coil (no soft iron ends).	9
Source:	Adapted from [9]	9
Fig. 8.	Coil and RLC meter for characterizing the soft iron ends	13
Fig. 9.	CAD of the soft iron end showing its cylindrical shape	13
Fig. 10.	Fabrication of a soft version of soft iron ends. The aim is to optimize for permeability and the tradeoff is flexibility. The type of elastomer partly determines the flexibility and the particle sizes partly determine the permeability.	14
Fig. 11.	CAD of the flexible soft coil with 30 turns and 10 mm diameter.....	14
Fig. 12.	The aim is to decrease the number of turns and the tradeoff is the amount of current. Additionally, I ² R losses limits the maximum amount of current that can flow through the wire without damaging it.	14
Fig. 13.	RLC model of the coil and a capacitor for generating a high transient current.	15
Fig. 14.	(a) (left) Flexible NdFeB magnet (b) (right) Flexible AlNiCo Magnet.....	16
Fig. 15.	Flexible NdFeB and AlNiCo placed adjacent to each other. An EPM assembly with these prototypes will have them arranged adjacently as shown.	16
Fig. 16.	Permanent magnet composed of Ecoflex, AlNiCo and NdFeB particles	16
Fig. 17.	When fabricating the flexible magnetic cores, the aim is to optimize for magnetic force and the tradeoff is flexibility. The volume ratio of the particles in the mixture is directly proportional to the exerted force but inversely proportional to the flexibility.	16
Fig. 18.	Images of ferroelastomer sample #20 from appendix IX and X showing the top view and side view of the samples. The ruler is included for scale.....	17
Fig. 19.	ARE-310 Thinky mixer configured to mix the mixtures of iron particles and Ecoflex at 2000 rpm for 30 seconds... ..	17
Fig. 20.	CAD of mold used to fabricate ferroelastomer samples.....	17
Fig. 21.	Elcometer 4340 Automatic Film Applicator is used to create a thin layer of Ecoflex that is then used to make a shell to contain iron particles.....	18
Fig. 22.	CAD of particle in a shell mold	18
Fig. 23.	Extracting a thin ecoflex film of about 20mm by 80mm	18
Fig. 24.	Ecoflex film layed on the inner surface of one half of the mold	18
Fig. 25.	Pouring some ecoflex 30 into the assembled mold to seal the bottom end of the mold	18
Fig. 26.	Pouring iron particles into the mold and sealing the top with ecoflex.....	19
Fig. 27.	Mold sealed with Ecoflex 30 and then placed in a vacuum chamber to evict the air. The bubbles observed are due to air escaping from the inside of the shell. Note that the Ecoflex at the top is yet to cure.	19
Fig. 28.	Two shells joined with “wings”	19
Fig. 29.	Tools used to parted the cojoined shells	19
Fig. 30.	Fabrication procedure for flexible coil[11]. A) Ecoflex rolled on a flat surface. B) Micro rod rolled on Ecoflex surface. C) Placing coated rod on a hot plate to cure the Ecoflex. D) Removal of the carbon rod and injection of EGaIn so as to make the tube conductive. Electrodes are inserted at the ends to provide electrical contact points. E) Roll tube into coil F) Embedding coil in a silicon layer.....	20
Source:	Adapted from[11]	20
Fig. 31.	Injecting EGaIn into a silicone tube using a syringe	20
Fig. 32.	CAD of mold for winding coil(left) and a 3D printed version(right)	20
Fig. 33.	Coil prototype I (left) and III(right)	20
Fig. 34.	Coil prototype IV side view	20
Fig. 35.	Coil prototype IV isotmetric view	21
Fig. 36.	CAD of halbach array container for magnets. A halbach array is used to create a homogenous magnetic field to prevent the magnetic particles from clustering or drifting.....	21

Fig. 37.	Assembled halbach array used to create a homogenous magnetic field to prevent the magnetic particle from clustering or drifting.....	21
Fig. 38.	ASC SCIENTIFIC impulse magnetizer(Model IM-10-30).....	21
Fig. 39.	F.W BELL 5180 Gauss/Tesla meter being used to characterize a fabricated magnetic sample made out of strontium ferrite and Ecoflex 30.....	22
Fig. 40.	Effect of increasing the percentage of iron on the inductance of the sample. The volume ratio refers to absolute volume ratio of iron. The blue line at the very top corresponds to the values of a shell filled with just iron filings. The red line at the bottom corresponds to the values of the coil with no core (ie. air core). Error bars are derived from the standard deviation.....	22
Fig. 41.	Effect of increasing the percentage of iron on the inductance of the sample. The volume ratio refers to absolute volume ratio of iron. The blue line at the very top corresponds to the values of a shell filled with just iron filings. The red line at the bottom corresponds to the values of the coil with no core (ie. air core). Error bars are derived from the standard deviation.....	22
Fig. 42.	Effect of increasing the percentage of iron by mass on the inductance. The mass ratio refers to absolute mass ratio of iron. Error bars are derived from the standard deviation.	23
Fig. 43.	Effect of increasing the percentage of iron by mass on the relative permeability. The mass ratio refers to absolute mass ratio of iron. Error bars are derived from the standard deviation.	23
Fig. 44.	Effect of vacuuming samples on the relative permeability of 300-micron particle samples. Plotted against absolute volume ratio of particles.	23
Fig. 45.	Effect of vacuuming samples on the relative permeability of 300-micron particle samples. Plotted against absolute mass ratio of particles.	23
Fig. 46.	Raw data plot of force against time and extension time for ferroelastomer sample 10.....	24
Fig. 47.	Box plot of the compliance of two ferroelastomer samples (sample 10 and sample 11) and one particle in a shell sample(mesh20shell#1). The middle line indicates the median of the measurements.	24
Fig. 48.	Plot of current against time for prototype IV coil.....	25
Fig. 49.	Sweeping number of turns and tube diameter while computing the maximum current.	25
Fig. 50.	Iterating over number of turns and tube diameter while computing the magnetic field strength(H).	26
Fig. 51.	Concept image of the assembled EPM. The particle in a shell soft iron ends are placed adjacent to the coil. There is no magnetic core in the center of the coil in this image.	26

Soft EPMs: Design and Fabrication of Soft Composite Materials for Soft Electro-magnetic Actuators

Billy Koech
Electrical Engineering

Harvard School of Engineering
and Applied Sciences

Cambridge, MA United States of
America

bkoech@college.harvard.edu

Abstract— Electromagnetic actuators are gaining momentum in soft robotic systems due to their small design footprints. Ferromagnetic and magnetic material are widely used in such actuators examples of which are electric motors, electromagnets, and electro-permanent magnets. With a focus on electro-permanent magnets due to their low power consumption, this project strives to fabricate and characterize soft magnetic and ferromagnetic materials that enable fabrication of soft electromagnetic actuators. Target applications include aiding motion (moving robot subcomponents around) and control (as an actuator acting on the environment) in soft robotics. This project is focused on designing and fabricating soft composite materials that can be used in the construction of an EPM; soft subcomponents of EPMs are designed to hold electro-magnetic properties similar to those of rigid EPMs. Quantitatively, the target properties include a holding force of 1.7N for a 10-millimeter scale device with compliance (flexibility) in the range of 0.001 to 0.05 GPa. Such compliance would enable the device to adapt to irregular non-planar surfaces that the rigid EPM could not. Measurement of the materials' compliance and magnetic properties are taken to characterize their performance.

Keywords—*Electropermanent magnet, permeability, coercivity, Ecoflex, compliance, coercivity, holding force, bistable.*

I. INTRODUCTION

Soft robotics is an emerging field with application in domains ranging from the medical industry to the food processing industry. Traditional methods for implementing soft actuators include pneumatic, shape memory alloys, dielectric-electro activated polymers and magnetic/electromagnetic methods. Of these methods, the most common ones are pneumatic[1] and electromagnetic methods. However, pneumatic methods require additional extensive pressure networks[2] for higher precision control[3], while most electromagnetic methods exist in rigid form[4] and require constant currents to maintain their magnetic field[5]. The cost for manufacturing and power increases for the former and latter methods respectively.

Therefore, there is a need for a soft actuator system that allows for high precision control at lower energy costs. This is the motivation of this project: to push the limit of compliance in energy efficient electromagnetic actuators by building a soft electropermanent magnet(EPM).

A. Problem Statement.

Pneumatic and electromagnetic methods are the most common methods of actuation in the field of soft robotics, however, pneumatic methods require extensive pressure networks in order to achieve high precision control, while electromagnetic methods require constant current flow in order to maintain the magnetic field.

The aim of this project is therefore to design and build an actuator that is compatible with soft robots and has less energy costs in comparison to current common methods.

B. Stakeholders

Soft electropermanent magnet actuators can be used to aid motion and control in soft robotics. This makes them applicable to current soft robotic systems that could use a soft latching mechanism.

Pushing the limit of Compliance: While soft robotics has applications in the medical and industrial domains, the exact specification and needs in these fields vary but there is always need for high precision, reliable performance and higher compliance. The wider soft actuator research community will benefit from the composite materials designed here because the empirical studies on these materials show the limits to which compliance could potentially be pushed in EPM actuators.

The target client for this project more specifically is Self-Organizing Systems Research(SSR) Group. Researchers in this group are always looking for methods of building systems that can self-assemble to execute larger tasks that could not be completed by individual agents. The actuator developed in this project would essentially enable a system of multiple agent to latch onto one another. Below is a map showing the key stakeholders:

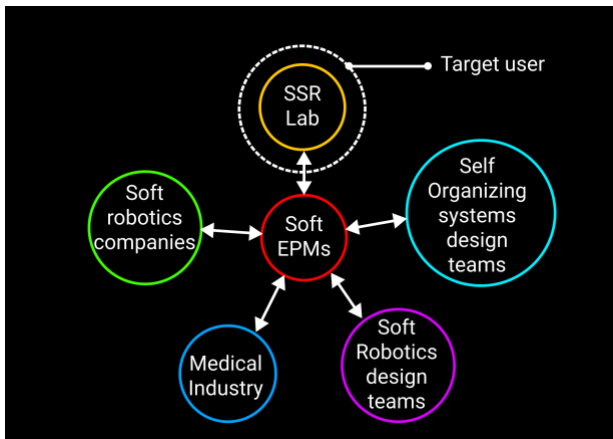


Fig. 1. Stakeholder map. SSR: Self Organizing Systems Research

The diagram below shows where the project exists as part of larger robotic system:

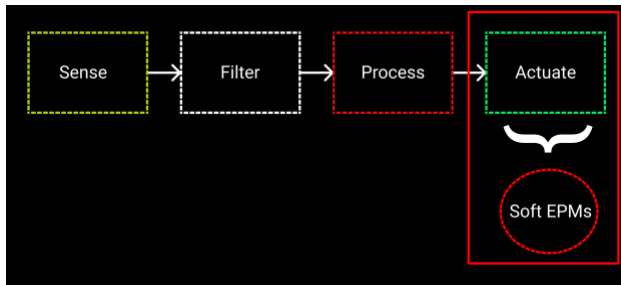


Fig. 2. System diagram showing the where soft Electropermanent magnet (EPM) actuators reside in a larger system.

Other electromagnetic devices that could leverage soft composite materials in their designs include motors, relays, electromagnetic valves, moving iron actuators, moving coil actuators and electromagnetic locks to name some of them.

II. BACKGROUND RESEARCH

A. Characterization of magnetic materials

Magnetic materials are primarily characterized using a B-H graph which shows the variation of the induced magnetic flux density in the materials (B) against the applied magnetic field strength(H). From the B-H graph quantities such as remanence, coercivity, saturation induction and permeability can be derived. The definitions for these terms are provided in this section.

Remanence: This is the residual magnetism left behind when the external magnetic field producing the magnetizing force H is removed. It is denoted by B_r . It corresponds to the positive or negative y-intercept of the B-H graph.

Saturation induction: This is a measure of the maximum attainable magnetic flux density of a material; it is achieved by applying a magnetizing force on a material up to a point where further magnetization is not possible. In the case of the B-H graph it corresponds to the levelling off of the graph; it is denoted by B_s .

Coercivity: This is a measure of the resistance of a material to change its magnetization. It is quantified by the intensity of the magnetic field strength needed to reduce the magnetization of a material to zero after the sample has been driven to saturation. It is denoted by H_c and corresponds to the x intercept in the second quadrant of the B-H graph. Even though values in the second quadrant are negative, coercivity is usually expressed as a positive value.

Permeability: This is a measure of the ease with which a magnetic domain can form in a material. Absolute permeability is defined as the ratio of the magnetic flux density(B) to the magnetic field strength H. Consequently, it can be derived from the B-H graph by finding the slope of the curve. When the absolute permeability is divided by the permeability of vacuum it yields the relative permeability.

B. Magnetic Material Types

Paramagnetic materials: These are materials that are weakly magnetized when placed in an external magnetic field. The direction of magnetization is the same as the applied field thus they reinforce the applied field[6]. They are found to exhibit relative permeabilities close to 1 but slightly greater and have linear B-H graphs[6]. They include metals such as aluminum, gold, manganese and platinum. Fig. 3 shows the B-H graph of paramagnetic materials

Diamagnetic materials: These are also materials that are weakly magnetized when placed in an external magnetic field. They differ from paramagnetic materials by the direction of magnetization: the direction is opposite to that of the applied field in accordance with Len'z Law. Examples include bismuth, mercury, silver, and copper. They are also found to have relative permeability close to 1, but slightly less and linear B-H graphs[6]. Fig. 3 shows the B-H graph of diamagnetic materials.

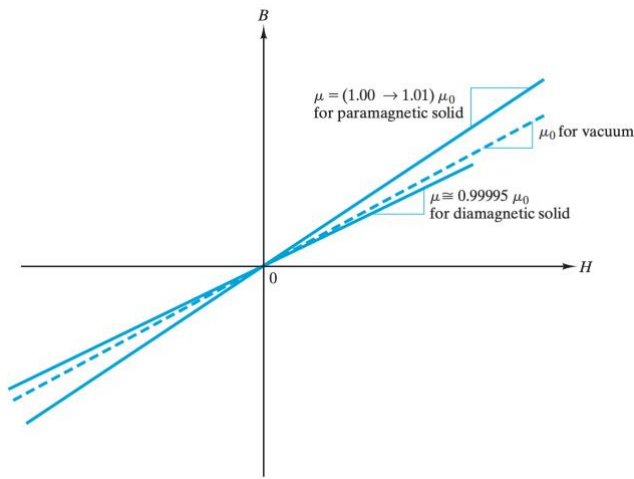


Fig. 3. Example B-H graph of diamagnetic and paramagnetic materials.

Source: Adapted from [6]

Ferromagnetic materials: These are materials that are strongly magnetized when placed in an external magnetic field. They generally exhibit strong interactions with magnetic fields. The name is derived from the term *ferrous* which means iron-containing but there are non-iron elements that exhibit similar magnetic properties. Examples of ferromagnetic materials include iron, cobalt, nickel and many of their alloys. Ferromagnetic materials are characteristically identified by their B-H graph that increases dramatically with the field strength as shown in Fig. 4. The reversible path traced by the solid line will always be traced whenever the magnetizing force is cycled back and forth[6].

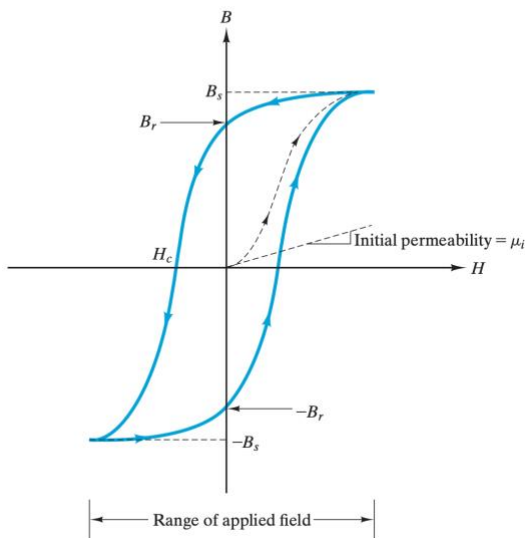


Fig. 4. Example B-H graph of a ferromagnetic materials.

Source: Adapted from [6]

Soft ferromagnetic materials: These are types of metallic ferromagnetic materials with high permeability but low coercivity relative to hard ferromagnetic materials. Coercivity is regarded to be the distinguishing quantity with most soft ferromagnetic materials being found to have a value much less than 100 A/m[7]. The B-H graph for soft ferromagnetic materials is shown in Fig. 5

Hard ferromagnetic materials: These are types of metallic ferromagnetic materials with high remanence and high coercivity relative to soft ferromagnetic materials. As with soft ferromagnetic materials, coercivity is the main distinguishing factor for hard ferromagnetic materials; most are found to have coercivity above 100,000 A/m[7]. The B-H graph for hard ferromagnetic materials is shown in Fig. 5.

Semi-hard ferromagnetic materials: These are materials with intermediate coercivity between that of soft and hard ferromagnetic materials. Most are found to have coercivity between 1,000 and 100,000 A/m[7].

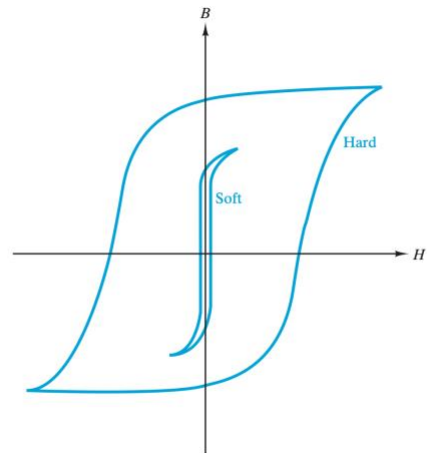


Fig. 5. Example B-H graph of soft and hard ferromagnetic materials.

Source: Adapted from [6]

Ferrimagnetic materials: These are materials with a crystal structure that leads to some antiparallel spin pairing which reduces the net magnetic moment below that possible in metals[6]. For example, a compound with iron ions in two ionic states (such as Iron(II) and Iron(III)) results in different ionic states with opposing magnetic momenta thus decreasing the magnetic strength in comparison to purely ferromagnetic materials[8]. The hysteresis curve in the B-H graph is similar to that of ferromagnetic materials except the saturation induction point is lower.

C. Electromagnets

An electromagnet consists of a conductive wire wrapped around a core. The flow of current in the wire generates a magnetic field on each turn which then combine to exert a net magnetic flux in a direction defined by the right-hand rule for solenoids. The magnetic field density (B) is proportional to the permeability of the core, the number of turns, the current in the coil, but inversely proportional to the length of the coil as shown in *Equation 1* below.

$$B = \frac{\mu N I}{l} \quad \text{Equation 1}$$

Where:

B - Magnetic field

μ - absolute

permeability of core

N - number of turns

I - amount of current

l - length of coil

The magnetic field strength is a function of just the number of turns, the current and the length as shown in *Equation 2* below:

$$H = \frac{N I}{l} \quad \text{Equation 2}$$

Where:

H - Magnetic field strength

N - number of turns

I - amount of current

l - length of coil

D. Electropermanent magnets

The rigid version of an EPM shown in Fig. 6 is explored in depth in Knaian's[4] doctorate thesis on programmable matter. A similar explanation is used below to describe the theory of operation of this device:

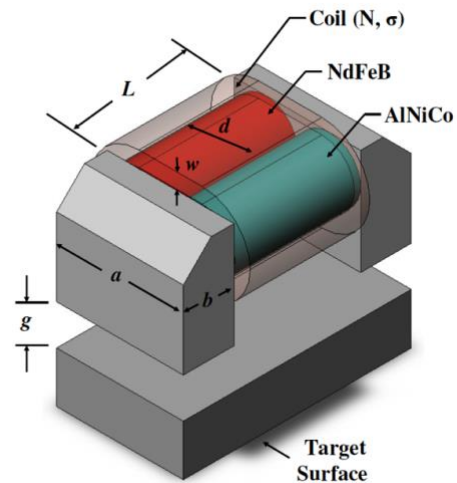


Fig. 6. Rigid version of an Electropermanent Magnet

Source: Adapted from [4]

The EPM in Fig. 6 consists of 4 main sub-components:

- Soft iron ends
- Semi-hard magnet (AlNiCo)
- Hard magnet (NdFeB)
- Coil

The coil is wrapped around the hard magnetic material (NdFeB) and a semi-hard magnetic material (AlNiCo). The ends are capped with soft iron bars. A current pulse in one direction magnetizes the semi-hard magnet; A pulse in the reverse direction reverses the polarity of the semi-hard magnet. If two adjacent poles of the magnets are in the same direction, then the two poles repel and all the magnetic flux is guided by the iron ends and flows through the metallic target surface in order to complete the loop. This provides the magnetic force that binds the target surface to the EPM. This is the ON state.

If the adjacent poles of the magnets are in opposite directions, then they attract and all the flux flows through the soft iron ends therefore closing the loop through the soft iron ends. The target surface is not attracted to the EPM. This is the OFF state.

Design and fabrication of a completely soft version of an EPM with the same number of components as the rigid EPM has not been successfully accomplished in published literature at the time that this is written.

Fabrication of a soft and miniaturized version of an EPM has been attempted by some researchers at the Ecole Polytechnique fédérale de Lausanne (EPFL) research institute[9]. Their method involves making just a flexible magnetic core. The principle of operation of their EPM also slightly differs from that described

¹ “Soft” refers to the magnetic property as opposed to the compliance

above because they do not use the soft iron ends to guide the magnetic flux. Instead the holding force is a sum of the net magnetization of a semi hard and a hard magnetic material as shown in Fig. 7 below. Still this project builds on their work by leveraging their recommendation for fabricating a flexible core. With this setup Raad[9] was able to achieve an EPM of dimensions 0.5x0.5x1.5mm with a holding force of 10mN.

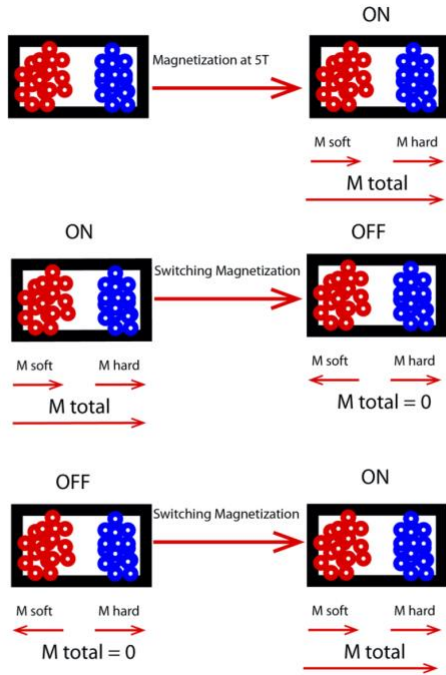


Fig. 7. Principle of operation of an EPM with just a semi-hard magnet, a hard magnet and a coil (no soft iron ends).

Source: Adapted from [9]

To improve on their work, they recommend mixing 5 μm grain size of NdFeB with 50 μm grain size of semi-hard magnetic powder.

The design of the switching circuit in this project is based on that of Knaian[4] and Haghghat's[10] designs of rigid EPMs. In Knaian's[4] design the EPM has a length of 6 mm and the coil is hooked up to a power supply of 20V that drives 5.3A current through the coil for about 20 μs . In Haghghat's[10] design a switching circuitry is designed to run on a 3.7V LiPo to power a 1mm EPM by driving 30A for 50 μs .

The design of the flexible coil is based on similar work done by Do et al.[11] where they fabricate an electromagnetic coil out of a conductive liquid metal alloy called Eutectic Gallium Indium (EGaIn) and silicone tubes.

E. Motivation for using EPMs

In this project the author made the design decision to focus on soft composite materials for just EPMs because EPMs are low energy devices with switching energy that scales with volume, and holding force that scales with area as proved by Knaian[4]. The higher the surface area to volume ratio the higher the energy efficiency. The scaling properties for EPMs is summarized in TABLE I. below.

TABLE I. SUMMARY OF SCALING PROPERTIES OF EPMs. ADAPTED FROM [4]

Symbol	Parameter	Length Scaling	Turns Scaling
F	Force	L^2	Const
I_{max}	Current	L	L^{-1}
R	Resistance	L^{-1}	N^2
V_{min}	Voltage	Const.	N
L	Inductance	L	N^{-2}
τ	Time Constant	L^2	Const.
T	Pulse Length	L^2	Const.
E	Pulse Energy	L^3	Const.

For the same reason, EPMs are chosen over pneumatic and other electromagnets- so as to reduce the energy demand.

III. DESIGN GOALS AND TECHNICAL SPECIFICATIONS

A. Goals

The primary goal of this project is to design and characterize all the components that are part of electropermanent magnetic actuators using soft composite materials.

Below are the fabrication sub-goals:

1. Fabricate compliant iron poles that are highly permeable.
2. Fabricate compliant semi-hard magnet (AlNiCo) with remanence comparable to that of a rigid EPM.
3. Fabricate compliant hard magnet (NdFeB) with equivalent remanence to that of the semi-hard magnet.
4. Fabricate a soft coil with high conductivity.
5. Assemble the EPM latch.
6. Characterize soft EPM and compare performance to a rigid version of the similar size.

The quantitative specifications for these sub goals are discussed in the next sections.

Given that an EPM's switching energy scales with the volume, while the holding force scales with the area, the first constraint to be established is the size of the device. Building a soft EPM is quite ambitious given that a fully flexible EPM is

unprecedented. To minimize the energy requirements while still setting an achievable goal the author chose the centimeter scale.

If one considers an EPM with residual induction of 0.5 T, and target surface of 3mm by 3mm, one obtains a force of 1.7N in accordance with Knaian's[4] holding force equation shown below in Equation 3.

$$F_{\text{holding}} = \frac{B_r^2 \times S_{\text{magnet}}}{\mu_0} \quad \text{Equation 3}$$

Where:
 F_{holding} – holding force
 S_{magnet} – surface area of magnet
 B_r – remanence
 μ_0 – vacuum permeability

The size and other specifications are further discussed and summarized in the following sections:

B. Device Size/Sacle

- **Quantitative Description:** Total length of 1cm or less.
- **Justification:** Previous versions of EPMs, developed by other researchers, have been able to attain lengths of 0.5mm[4] and 1cm[10]. This project focuses on the centimeter scale so as to reduce the energy demand. The surface area of the magnet surface is approximated to be 3mm by 3mm.
- **Measurement:** Length can be measured with a ruler.

C. Holding Force

- **Quantitative Description:** The aim is to achieve a holding force that is as close as possible to that of an equivalent rigid EPM. This project's target holding force is 1.7N.
- **Justification:** One paper shows that two EPMs of size 1cm attracting each other could achieve a holding force of 1.24N[10]
- **Measurement:** Holding force can be measured by attaching the soft EPM to a spring of known spring constant k and measuring the extension of the spring until the EPM detaches from the target surface. The force can be computed using the formula in Equation 4.

$$F = -k \times x \quad \text{Equation 4}$$

Where
 F – holding force
 k – spring constant
 x – extension

D. Soft Iron End Permeability

- **Quantitative Description:** Relative permeability equal to or greater than 10.
- **Justification:** The relative permeability of iron powder ranges between 14 and 100 [12]. A guide on soft magnetic material by Wulf Günther and Paul Winkler suggests that if the permeability is less than 500 then the flux begins to stray[13]: “In case of low materials permeability (<500) or gaps or certain core / winding designs, where the field and the flux is not guided by the magnetic material completely, the field and flux parts through air...”[13] The implications of this on the EPM iron ends is uncertain. Therefore, the effectiveness of the soft iron ends is left to be determined empirically.
- **Measurement:** Permeability can be calculated from the inductance of a material. Inductance can be measured by placing a coil of known turns N around a material and connecting the coil to an RLC meter. Equation 5 shows the relationship between inductance and permeability.

$$L = \frac{\mu_0 N^2 A}{l} \quad \text{Equation 5}$$

Where:
 L – inductance
 μ_0 – absolute magnetic permeability
 N – number of turns
 A – cross sectional area of coil
 l – length of coil

E. Soft Iron End Compliance

- **Quantitative Description:** The target range for compliance is between 0.001 and 0.05 GPa (Young's Modulus)
- **Justification:** Compliance is dependent on the substrate material used as a continuum medium for the particles. It is projected that the addition of soft iron particles

decreases the compliance, but the reported values for ferroelastomer mixtures is between 0.001 and 0.05 GPa[3].

- **Measurement:** Young's modulus can be measured by setting up an experiment to measure stress and strain[14]. Such measurements can be collected using an Instron device. The equation below shows the definition of Young's modulus:

$$E = \frac{F/A}{\Delta L / L} \quad \text{Equation 6}$$

Where:

E- Young's modulus

F- Force exerted

A- Area

ΔL – Change in length

L- Initial length

F. Hard Permanent Magnet Coercivity

- **Quantitative Description:** Coercivity is a measure a materials resistance to magnetization or demagnetization. The target coercivity for the hard-permanent magnets is about 1000kA/m
- **Justification:** N40 NdFeB is used in the implementation of the rigid EPM[4]. It's coercivity is about 1000 kA/m[15].
- **Measurement:** Coercivity of a material can be measured using a magnetometer, or a setup with a gauss meter for measuring the magnetic field density(B) and a magnetizer producing a magnetizing field strength(H). It can also be calculated from the B-H graph of the magnetic material as discussed in the background research section.

G. Hard Permanent Magnet Compliance

- **Quantitative Description:** The target range for compliance is between 0.001 and 0.05 GPa; this is similar to that of the soft iron ends.
- **Justification:** Reported values for ferro-elastomer mixtures is between 0.001 and 0.05 GPa[3].
- **Measurement:** Compliance can be measured by calculating Young's modulus. Refer to *Equation 6*.

H. Semi-hard Permanent Magnet Coercivity

- **Quantitative Description:** The target coercivity is 50 kA/m.
- **Justification:** AlNiCo is used in the implementation of the rigid EPM[4]. The coercivity of LNG40 AlNiCo (also known as AlNiCo V) is about 50 kA/m [16].
- **Measurement:** Coercivity of the semi-hard permanent magnet can be measured in a similar fashion to that of the hard permanent magnet- with a magnetometer, or a gauss meter in conjunction with a magnetizer, or just from the B-H graph.

I. Semi-hard Permanent Magnet Compliance

- **Quantitative Description:** The target range for compliance is between 0.001 and 0.05 GPa; this is similar to that of the soft iron ends.
- **Justification:** Reported values for ferro-elastomer mixtures is between 0.001 and 0.05 GPa[3].
- **Measurement:** Compliance can be measured by calculating Young's modulus. Refer to *Equation 6*.

J. Coil Conductivity

- **Quantitative Description:** The limit on the amount of current is determined by the properties of the conductive material used to make the coil. This project uses Eutectic Gallium Indium (EGaIn) which is a conductive liquid metal alloy that can be injected or embedded in channels. The literature value for its conductivity is $\sigma = 3.4 \times 10^6 \text{ Sm}^{-1}$ [17]. As with other conductors, it is subject to I^2R losses that dissipates in the form of heat. The conductivity together with the dimension of the wire and the chemical properties of the liquid metal alloy(EGaIn) will be used to determine the amount of current that can be driven through the wires without burning it out.
- **Justification:** Various researchers have attempted to make soft coils out of EGaIn, and they have reported conductivity with magnitudes of around $\sigma = 3.4 \times 10^6 \text{ Sm}^{-1}$. [11]–[13]
- **Measurement:** Conductivity is the reciprocal of resistivity. Resistivity can be calculated from the resistance of a material (measured using an ohmmeter), the cross-sectional area and the length of the conductor as shown in *Equation 7* and *Equation 8*.

$$\rho = R \frac{A}{L} \quad \text{Equation 7}$$

Where:
 ρ - resistivity
 R – resistance
 A - Area
 L - Length

$$\sigma = \frac{1}{\rho} \quad \text{Equation 8}$$

Where:
 ρ - resistivity
 σ – conductivity

K. Coil Magnetic field strength (H)

- **Quantitative Description:** Magnetic field of 100 kA/m
- **Justification:** The material used for the semi-hard permanent magnet (AlNiCo) has a coercivity of 50kA/m. In order to reverse its polarity, the magnetic field of the coil has to be greater than 50kA/m; hence a target value of 100kA/m should be sufficient.
- **Measurement:** Magnetic field strength(H) can be derived from magnetic field(B) of the coil as shown in Equation 9. Magnetic field (B) can be measured with a gauss meter.

$$H = \frac{B}{\mu} \quad \text{Equation 9}$$

Where:
 H – magnetic field strength
 μ - absolute magnetic permeability
 B – magnetic field

L. Coil transient current limit

- **Quantitative Description:** The coil should be able to pass about 20A without burning out from I^2R heat dissipation. This high transient current is necessary to generate a magnetic field that can reverse the polarity of the semi-hard permanent magnet.

- **Justification:** In one publication the researchers used a RLC circuit to drive 22A of current through a 32-turn coil made out of 26 AWG in order to reverse the polarity of the AlNiCo magnet[10].
- **Measurement:** Transient currents can be measured with an oscilloscope that has a current probe.

TABLE II. SUMMARY OF TECHNICAL SPECIFICATIONS

Specification	Target value
Device Scale	1 cm long
Holding Force	1.7 N
Soft Iron End relative permeability	10
Soft Iron End compliance	0.001 to 0.05 GPa
Hard Permanent Magnet coercivity	1000 kA/m
Semi-hard Permanent coercivity	50 kA/m
Semi-hard Permanent magnet compliance	0.001 to 0.05 GPa
Coil conductivity	$3.4 \times 10^6 \text{ Sm}^{-1}$.
Coil magnetic field strength	100 kA/m
Coil transient current limit	20 A

IV. TECHNICAL DESIGN APPROACH

As shown in section III, a soft EPM consists of 4 different component each with their own specifications. Given that none of these subcomponents are available commercially (or in prefabricated form), they have to be designed and fabricated from raw materials. Converting each component to a soft flexible form is a large feat on its own therefore the project is split into three alternatives in order of increasing total flexibility. The term “latch” in the sections that follow is used to refer to a fully assembled device.

A. Latch Flexibility alternatives:

- **Flexible Iron Ends:** This alternative entails just converting the iron ends into flexible form but leaving every other component in rigid form. The soft iron ends are the main point of contact between the target surface and the latch therefore flexible iron ends might be sufficient to allow the device to adapt to irregular surfaces.
- **Flexible Iron ends and Coil:** This alternative involves converting the iron ends and the coil to flexible form. The permanent magnets retain their rigid form.
- **Fully Flexible device:** This alternative entails converting the iron ends, coil and permanent magnets

into flexible form. In theory such a device would have the highest possible compliance in comparison to the other alternatives.

TABLE III. below summarizes the advantages and disadvantages of each alternative.

TABLE III. COMPARISON OF ALTERNATIVES

Alternative	Advantage	Potential constraints/Disadvantages
Flexible Iron End	The soft iron ends are the main point of contact therefore the device can adapt to rigid planar surfaces and some non-planar surfaces	Compliance is limited to just one component. Difficult to latch onto highly irregular target surfaces
Flexible Iron ends and coils	More compliance in comparison to the previous alternative. The Young's modulus of the central region is higher than the previous alternative.	The additional compliance is still impeded by the rigid permanent magnets around which the coil is wound
Fully flexible device	Maximum attainable compliance would allow the full device to adapt to highly irregular non-planar target surfaces	Acquiring magnetic particles and fabricating with magnetized particles is industrially challenging and would require specialized equipment such as a halbach array and a ball mill.

The objective of this project is it push the limit of compliance therefore the third alternative would suite this objective. However, the occurrence of the 2020 COVID-19 pandemic placed more constraints on acquiring materials and access to laboratories for fabrication of the flexible permanent magnets. What this meant for the project is that only a portion of the third alternative could be achieved, and this is further discussed in the fabrication and measurements section.

B. Soft Iron End Design: Permeability-Flexibility trade off

Geometry Design: In order for the iron ends to be characterizable they have to be able to fit a coil of 10 mm diameter and 200 turns which is used to measure the inductance of the flexible iron end sample as shown in Fig. 8.

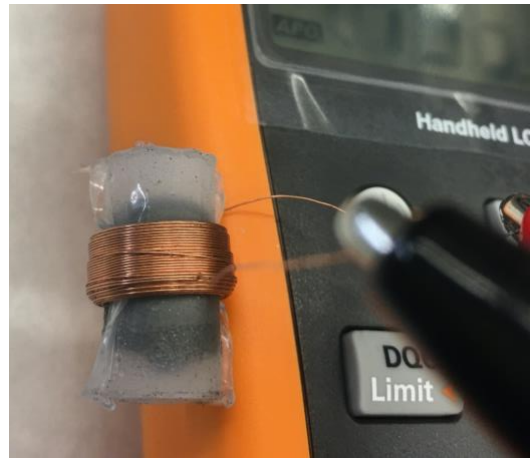


Fig. 8. Coil and RLC meter for characterizing the soft iron ends

This method of characterization therefore drove the design for the shape of the iron end as shown in Fig. 9.

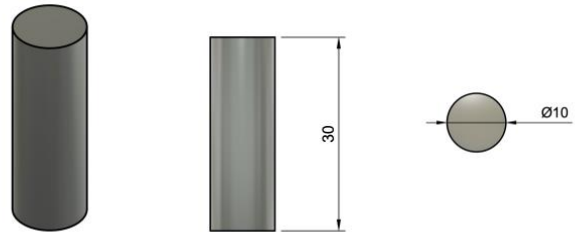


Fig. 9. CAD of the soft iron end showing its cylindrical shape

Design for flexibility: Fabrication of a flexible iron ends involves combining iron particles with an elastomer in order to attain flexibility while preserving the high permeability property of iron. Two fabrication processes are designed both of which are discussed in the prototyping section. The first alternative is mixing iron particles with an elastomer. The second involves creating an elastomeric shell into which particles can be embedded; the latter attains flexibility because the particles in a shell can move and adapt to any shape.

Both of these methods have an associated *permeability-flexibility trade off*: The volume ratio of iron in the mixture is proportional to the permeability and inversely proportional to the flexibility. The size of the particles also factors into the permeability and this relationship is discussed in the measurement/verification section. Fig. 10 summarizes the factors at play in the fabrication of the flexible iron ends:

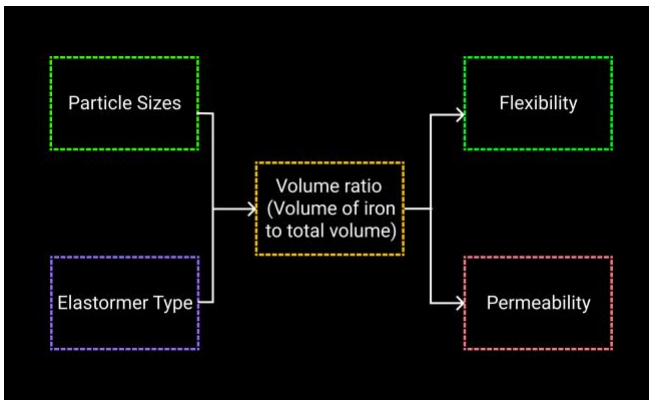


Fig. 10. Fabrication of a soft version of soft iron ends. The aim is to optimize for permeability and the tradeoff is flexibility. The type of elastomer partly determines the flexibility and the particle sizes partly determine the permeability.

C. Soft coil Design: Current-Turns trade off

Geometry Design: The coil should be able to wrap around the permanent magnet cores with enough turns to generate a magnetic field strength H of 100kA/m. The design in Fig. 11 shows a coil of 30 turns and 10 millimeters diameter. The geometry of the coil is similar to that of a cylindrical solenoid.

The number of turns is subject to change based on the first prototype from which actual values of resistivity and inductance of the coil are determined. This design adjustment is shown in the measurements section.



Fig. 11. CAD of the flexible soft coil with 30 turns and 10 mm diameter

Design for flexibility: Copper wire is already flexible but once wound into turns it becomes inflexible. This necessitates the need for a more flexible coil: the coil design involves a flexible tube into which conductive liquid metal alloy is injected. Two alternatives are developed and explored in the prototyping section: the first involves injecting Eutectic Gallium Indium (EGaIn) into a self-fabricated or purchased silicon tube [11]. The second involves mixing silver nano wires with an elastomer in order to attain a conductive elastomeric wire. The fabrication procedure for each of these alternatives is discussed in the prototyping section.

The objective while fabricating the coil is to decrease the number of turns so as to meet the size specification while not

compromising on the amount of magnetic force generated; the tradeoff for decreasing the turns is increase in the required amount of current needed to generate an equivalent magnetic flux density as shown in Equation 10:

$$B = \frac{\mu N I}{l} \quad \text{Equation 10}$$

Where:
 B - Magnetic flux density
 μ - absolute permeability
 N - number of turns
 I - amount of current
 l - length of coil

The amount of current that can be passed through the wire also has a limit defined by the resistance of the wire and its inductance when wound into a coil; high currents generally have the tendency to burn wires due to heat energy dissipation in the form of I^2R losses. The relationships discussed above are summarized in Fig. 12:

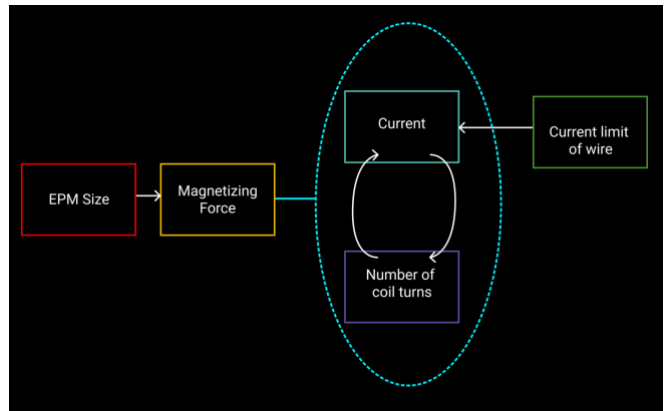


Fig. 12. The aim is to decrease the number of turns and the tradeoff is the amount of current. Additionally, I^2R losses limits the maximum amount of current that can flow through the wire without damaging it.

Design to prevent burning out from a high transient current: Generation of the magnetic flux needed to reverse the polarity of AlNiCo is through pulse magnetization where a capacitor is discharged on the coil to generate a high transient current. This project borrows from a design by other researchers where they attained 30A for 50 microseconds [10]. The current limit for EGaIn is not specified in literature therefore this will have to be determined empirically by having a setup that drives a high current while measuring effects on the conductivity of

the wire. This setup is discussed in detail in the measurements section.

The coil can be modelled as an RL component where the resistance is determined by the conductivity of EGaIn, its length and cross-sectional area as shown in equation *Equation 11*; the inductance can be determined from the permeability of the core, the number of turns, the length, and the cross section of the coil as shown in *Equation 12*.

$$R = \frac{\rho \ell}{A} \quad \text{Equation 11}$$

Where:
R - resistance
ℓ - length of wire
ρ - resistivity of EGaIn
A - cross sectional area of wire

In order to generate a high transient current, a capacitor is discharged on the coil. The combination of the coil and the capacitor can be modelled as a series RLC circuit as shown in Fig. 13.

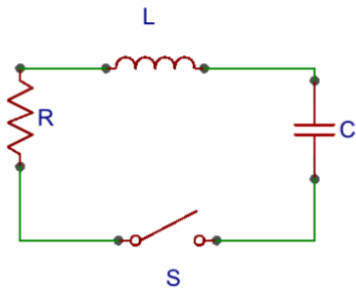


Fig. 13. RLC model of the coil and a capator for generating a high transient current.

$$L = \frac{\mu N^2 A}{\ell} \quad \text{Equation 12}$$

Where:
L - inductance
ℓ - length of coil
N - number of turns
A - cross sectional area of coil (not wire)
μ - permeability of core

Based on the value of the resistance and inductance, a suitable capacitor can be chosen and the current computed using the RLC series current equations: If $R^2 < \frac{4L}{C}$ then the circuit is underdamped and *Equation 13* gives the current.

$$\omega_0 = \sqrt{\frac{1}{LC} - \left(\frac{R}{2L}\right)^2}$$

$$i(t) = \frac{V_0}{\omega_0 L} e^{-\frac{Rt}{2L}} \sin \omega_0 t \quad \text{Equation 13}$$

If $R^2 > \frac{4L}{C}$ then the circuit is overdamped and *Equation 14* gives the current.

$$\omega_0 = \sqrt{\left(\frac{R}{2L}\right)^2 - \frac{1}{LC}}$$

$$i(t) = \frac{V_0}{\omega_0 L} e^{-\frac{Rt}{2L}} \sinh \omega_0 t \quad \text{Equation 14}$$

If $R^2 = \frac{4L}{C}$ then the circuit is critically damped and *Equation 15* gives the current.

$$i(t) = \frac{V_0 t}{L} e^{-\frac{Rt}{2L}} \quad \text{Equation 15}$$

D. Flexible permanent magnet design: Force flexibility trade off

Geometry design: Two alternatives are ideated for the geometry of the permanent magnets. The first resembles the rigid version of the EPM where each permanent magnet is fabricated from a mixture of magnetic particles and an elastomer then molded into a cylinder. In this design each permanent magnet exists as a separate cylinder from the other, but they are placed adjacent to each other in the final assembly. Fig. 14 and Fig. 15 show the CAD for the first permanent magnets prototype design.

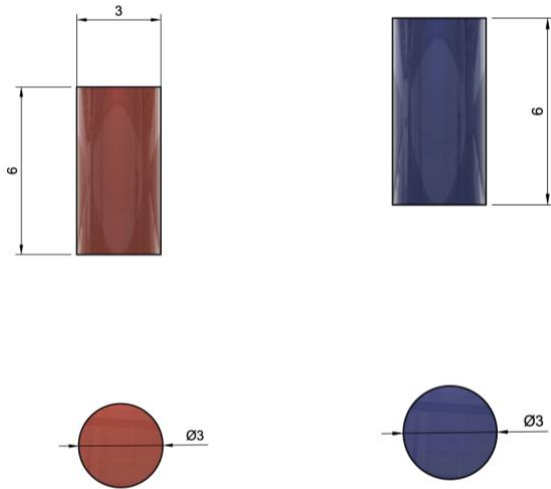


Fig. 14. (a) (left) Flexible NdFeB magnet (b) (right) Flexible AlNiCo Magnet

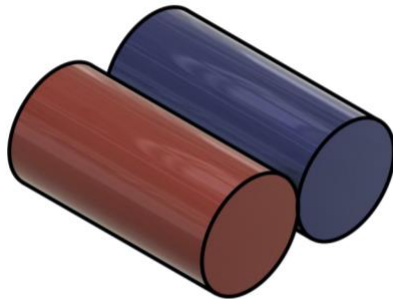


Fig. 15. Flexible NdFeB and AlNiCo placed adjacent to each other. An EPM assembly with these prototypes will have them arranged adjacently as shown.

The second design (shown in Fig. 16) involves mixing both magnetic particles (NdFeB and AlNiCo) with an elastomer to create one homogenous mixture. The mixture would then be cured in a mold to arrive at a geometry shown in Fig. 16. The edges are curved to ensure that a coil wrapped around it is in flush with the surface. Some researchers at EPFL attempted to create such a magnet by mixing NdFeB and AlNiCo particles with an elastomer [9]. They recommended using $5 \mu\text{m}$ grain size for NdFeB and $50 \mu\text{m}$ of semi-hard magnetic powder to yield a high filling factor [9]. This design follows those recommendations.

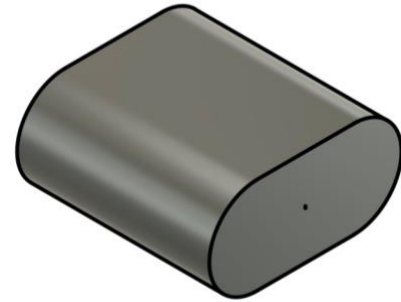


Fig. 16. Permanent magnet composed of Ecoflex, AlNiCo and NdFeB particles

Design for flexibility: Unlike the soft iron ends, magnetic particles cannot be fabricated using the particles in a shell method because the individual particles would be free to move in the shell; that is, an applied magnetic field would change the orientation of the particles rather than change their polarity. For this reason, only one design is proposed: Mixing the particles with an elastomer to create a homogenous mixture. Once such a mixture has cured the individual particles will not be able to change their orientation, but the sample as whole should be able to bend thereby achieving flexibility. *The volume ratio of the magnetic particles in the mixture is proportional to the magnetic force and inversely proportional to the flexibility;* this is the trade off when designing the magnetic cores and it is summarized in the illustration in Fig. 17.

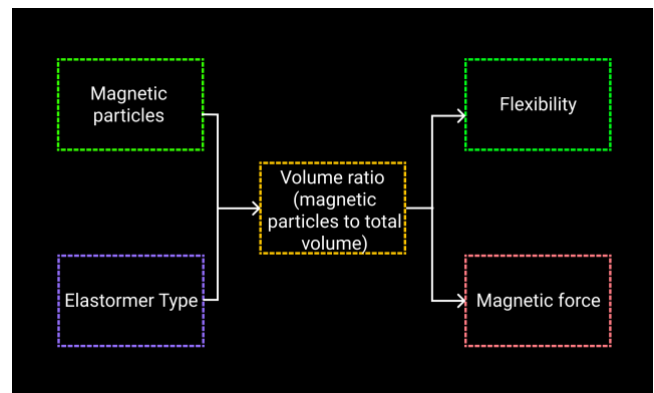


Fig. 17. When fabricating the flexible magnetic cores, the aim is to optimize for magnetic force and the tradeoff is flexibility. The volume ratio of the particles in the mixture is directly proportional to the exerted force but inversely proportional to the flexibility.

V. BUILDING/PROTOTYPING

A. Soft Iron End Prototype

Two alternatives for designing the soft iron ends are ideated in the design section: the first is mixing iron particles of different sizes with an elastomer (*ferroelastomer* alternative); and the second is enclosing particles in a shell (*particle in a shell* alternative). Both alternatives are explored and the best of the two chosen. The results show that the particles in a shell alternative has higher permeability than the ferroelastomer alternative for samples fabricated with the same grain sizes. However, the fabrication procedure for the ferroelastomers and the data is still included here because it presents interesting findings on the behavior of iron when mixed with an elastomer. The fabrication procedures are discussed below:

Ferroelastomer fabrication methodology: The samples are fabricated by mixing an elastomer (Ecoflex 30) with iron particles of different sizes at different mass and volume ratios. Ecoflex 30 was chosen because it offers the highest possible compliance in comparison to Ecoflex 20 and 10. Below are the particle sizes used to fabricate samples in decreasing size:

- Iron 12 (300 microns)
- -70 mesh (210 microns)
- -20 mesh (100 microns)
- 6-10 microns
- 1-4 microns

The samples are fabricated by mixing iron particles with Ecoflex 30 in increasing volume ratios of iron particles. The first step starts with pouring a predetermined volume of iron particles in a plastic cup and measuring the mass. This is followed by adding Ecoflex 30 part A into the same plastic cup. An equivalent amount of Ecoflex 30 part B is then poured into the same cup. The mixture is then mixed in an ARE-310 Thinky mixer. Most of the samples are mixed at 2000 revolutions per minute (rpm) for 30 seconds as shown in Fig. 19. The mixture is then poured into a mold with holes of 10mm diameter (shown in Fig. 18 and Fig. 20) and placed in a 60°C oven for about an hour (or more for other samples). The molds were designed so as to fit the characterizing coil mentioned in the design section. A table with all the parameters used in the design of this experiment as well as the results is provided in appendix IX and X. Images of the sample are also available in a git repository provided in the references [18]. The measurement section discusses the implications of the measured sample permeabilities.

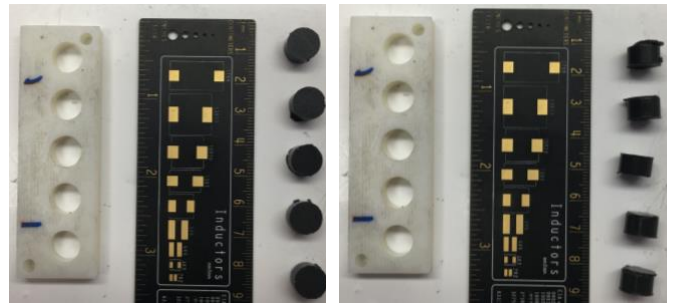


Fig. 18. Images of ferroelastomer sample #20 from appendix IX and X showing the top view and side view of the samples. The ruler is included for scale.

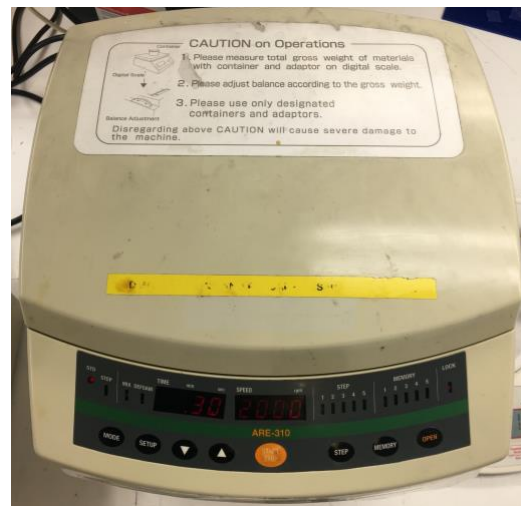


Fig. 19. ARE-310 Thinky mixer configured to mix the mixtures of iron particles and Ecoflex at 2000 rpm for 30 seconds.



Fig. 20. CAD of mold used to fabricate ferroelastomer samples.

Particle in a shell fabrication methodology: The samples are fabricated by enclosing particles in an elastomeric shell. It starts with the creation of a thin layer of Ecoflex 30 using a thin film applicator (Elcometer 4340 Automatic Film Applicator) shown in Fig. 21. The resulting film has a thickness of 0.3 millimeters.



Fig. 21. Elcometer 4340 Automatic Film Applicator is used to create a thin layer of Ecoflex that is then used to make a shell to contain iron particles.

The film is then cut into strips of about 20mm by 80mm as shown in Fig. 23. These dimensions are chosen so as to fit a mold designed to create a shell out of these layers. This mold is shown in Fig. 22.

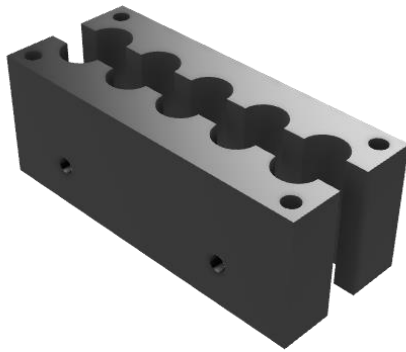


Fig. 22. CAD of particle in a shell mold

A very thin layer of Vaseline is applied onto the inner surface of these molds to prevent the Ecoflex strips from sticking onto the surfaces when demolding. The Ecoflex strip is then laid on the inner surface of the mold such that the strip is in flush with the curving surfaces as shown in Fig. 24. Uncured Ecoflex is then poured on the surface to act as an adhesive agent; two mirrored halves of the molds are then assembled and secured using nuts and bolts. A bottom layer for the mold is then attached and also fastened in place using nuts and bolts. Some Ecoflex is then poured from the open side of the mold. The purpose of the poured Ecoflex is to seal one end of the cylindrical shells as shown in Fig. 25.

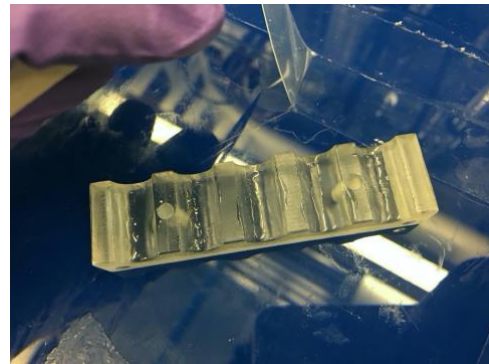


Fig. 23. Extracting a thin ecoflex film of about 20mm by 80mm



Fig. 24. Ecoflex film layed on the inner surface of one half of the mold

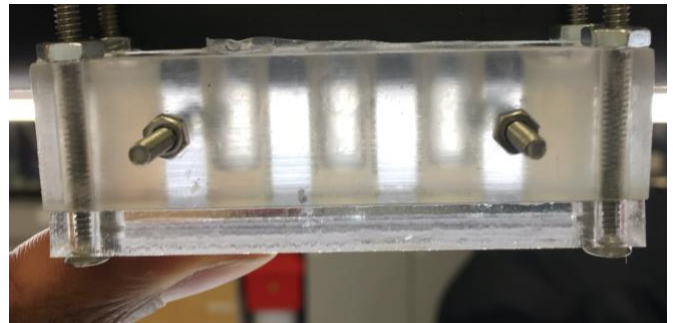


Fig. 25. Pouring some ecoflex 30 into the assembled mold to seal the bottom end of the mold

The mold is then placed in a 60°C oven for 1 hour to cure the Ecoflex. Once it has cured, it is removed, and iron particles are poured into the holes leaving about a 3mm space at the top for sealing the shell (Fig. 26). The top is sealed by pouring Ecoflex and leaving it to cure in the oven again for 1 hour.

Some samples were placed in a vacuum chamber set to 100 KPa for one hour to evict all the air inside the shell. Fig. 27 shows one such mold after it has been removed from the vacuum chamber.

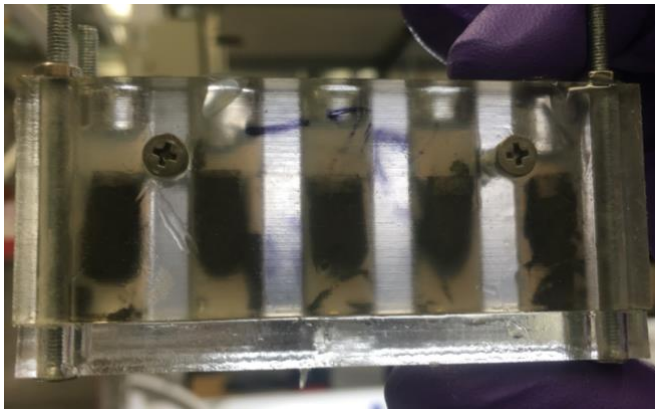


Fig. 26. Pouring iron particles into the mold and sealing the top with ecoflex

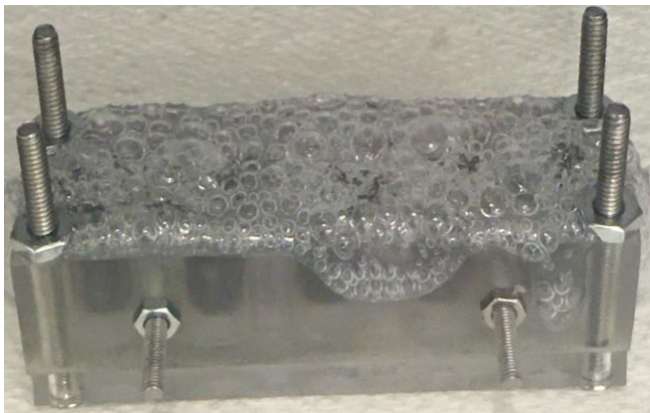


Fig. 27. Mold sealed with Ecoflex 30 and then placed in a vacuum chamber to evict the air. The bubbles observed are due to air escaping from the inside of the shell. Note that the Ecoflex at the top is yet to cure.

Once the samples have cured, the mold is taken apart by opening the nuts and bolts. The different samples are then separated by cutting across the “wings” joining the samples with a scalpel:

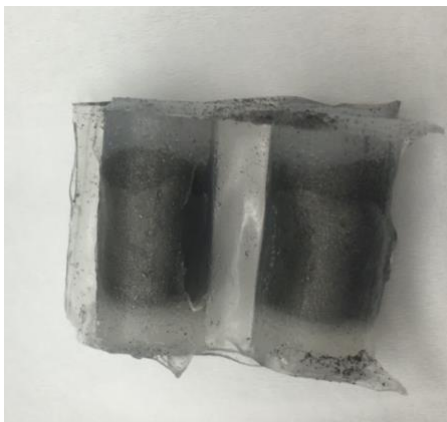


Fig. 28. Two shells joined with “wings”



Fig. 29. Tools used to parted the cojoined shells

After measuring the permeabilities of the vacuumed and non-vacuumed samples, it is noted that the non-vacuumed samples have higher permeabilities than the vacuumed ones. This is counterintuitive to the expectations of the author as one would expect tightly packed shells to have higher permeabilities. This still remains a mystery, and a discussion attempting to explain this is provided in the measurement/verify section. A table of all the fabricated samples and the measurements for the permeabilities is provided in appendix IX and X.

B. Soft Coil prototype

Two major prototyping alternatives were developed in the design section. The first is creating flexible wires by mixing silver nano wires with Ecoflex. The second is creating a silicone tube by either rolling a thin film of silicone or purchasing prefabricated silicon tubes into which EGaIn can be injected. The first alternative failed as the mixture of silver nano wires and Ecoflex lost its conductivity after curing. Therefore, this section details the procedure for fabricating the functioning alternative:

Silicone tube with EGaIn fabrication methodology: An attempt was made to create a tube by rolling a thin silicone film, but it proved too difficult to seal; furthermore, achieving a thin uniform diameter was a very difficult given the lack of a specialized high accuracy rolling device. Another option was to apply silicone on a carbon rod and remove the electrode after curing to remain with a tube like structure; this would be done in a fashion similar to that of Do et al.[11] in Fig. 30.

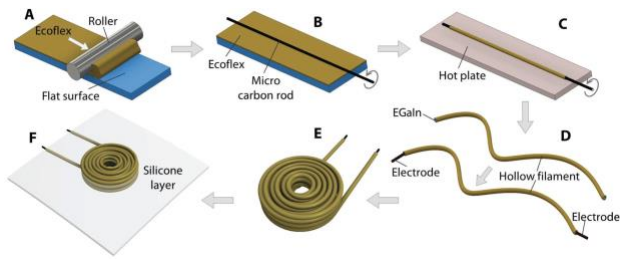


Fig. 30. Fabrication procedure for flexible coil[11]. A) Ecoflex rolled on a flat surface. B) Micro rod rolled on Ecoflex surface. C) Placing coated rod on a hot plate to cure the Ecoflex. D) Removal of the carbon rod and injection of EGaIn so as to make the tube conductive. Electrodes are inserted at the ends to provide electrical contact points. E) Roll tube into coil F) Embedding coil in a silicon layer.

Source: Adapted from[11]

However, this also proved to be challenging to control the thickness therefore a design decision was made to purchase prefabricated silicon tubes:

Tubes with two different inner diameters are purchased: 0.3mm and 0.5mm inner diameters. Each tube is injected with EGaIn using a syringe (30Ga syringe for the 0.3 mm tube and 27Ga syringe for the 0.5m) as shown in Fig. 31. A copper electrode is then inserted into the tube at each end . 28AWG and 22AWG wires proved to be thick enough to tightly fit into the 0.3mm and 0.5mm tubes respectively therefore not requiring any additional sealant. TABLE VIII. and TABLE IX. show the measurement results of the EGaIn Wire.

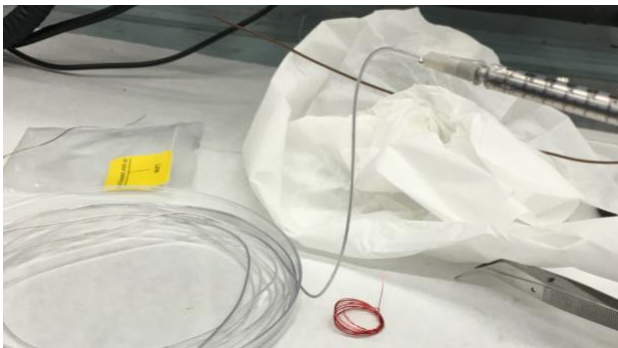


Fig. 31. Injecting EGaIn into a silicone tube using a syringe

After the wires are fabricated successfully Ecoflex 30 is poured onto the tube's outer surface(to act as an adhesive) before winding the wire on a 3D printed cylindrical mold of 10mm diameter. Vaseline is applied to the surface of the mold prior to winding for easy demolding.

Prototype I and III were wound successfully as shown in Fig. 33. Prototype II lost its ability to conduct before it was even wound due to a separation in liquid metal alloy channel.

Prototype I and III prototypes also lost their conductivity due to excessive stretching of the wire when wound around the mold.

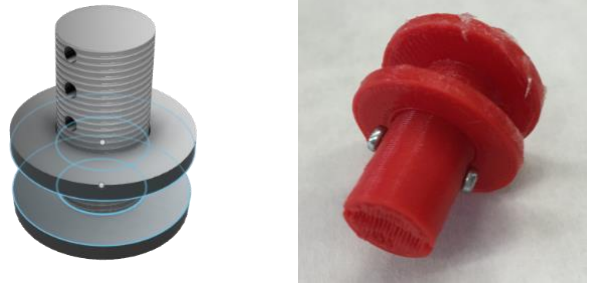


Fig. 32. CAD of mold for winding coil(left) and a 3D printed version(right)

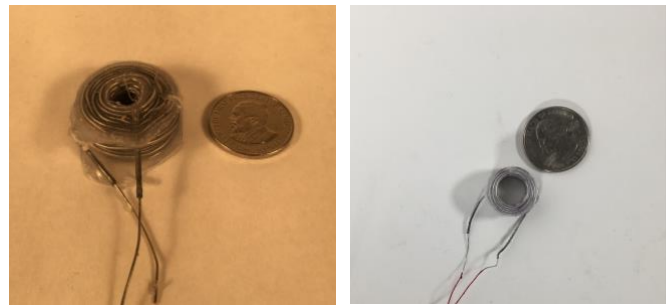


Fig. 33. Coil prototype I (left) and III(right)

A fourth prototype is therefore developed where the EGaIn is injected into the tube after the tube has been wound into a coil. This prototype worked better as the liquid metal alloy did not have any discontinuity in the channel thus it retained its ability to conduct. TABLE IX. shows the coil characteristics; Fig. 34 and Fig. 35 show its appearance.

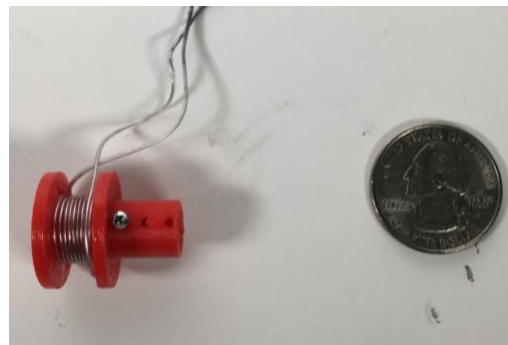


Fig. 34. Coil prototype IV side view

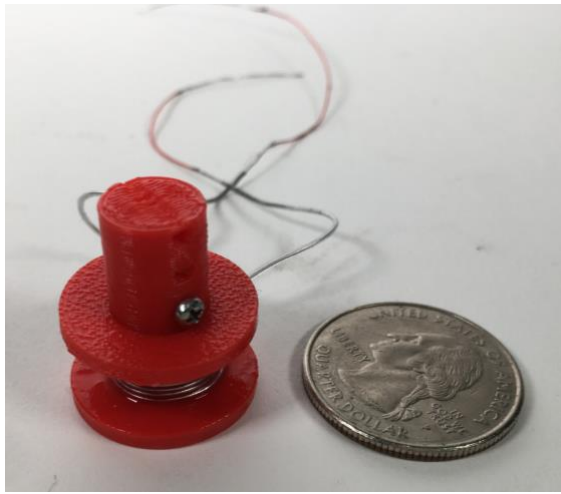


Fig. 35. Coil prototype IV isotmetric view

C. Magnetic core prototype

The magnetic core is fabricated by mixing magnetic particles with Ecoflex 30. Two prototyping procedures are proposed below: the first prototype—*separate bar* prototype—consist of two flexible cylindrical bars (one AlNiCo and the other one NdFeB) as mentioned in the design section; the second prototype—*singular integrated bar* prototype—consists of a single bar made from mixing together AlNiCo powder and NdFeB powder.

Acquiring magnetic particles proved to be challenging as most companies do not offer the required magnetic grades for this project (shown in the TABLE IV. below); other companies had lead times that exceeded the time scope of this project. Given this constraint the fabrication of the magnets is done with strontium ferrite powder just to prove the feasibility of the fabrication process.

TABLE IV. MAGNETIC PARTICLES GRADES. ADAPTED FROM [16]

Material	Grade	Coercivity (kA/m)	Remanence Br (T)
NdFeB	N40	1000	1.28
AlNiCo	LNG40	50	1.26

Separate bar fabrication methodology: The flexible bar sample is fabricated by mixing an Ecoflex 30 with strontium ferrite particles of size 25 μm . The mixture is mixed in the ARE-310 Thinky mixer at 2000rpm for 30 seconds. The mixture is then poured into a cylindrical mold and placed in a halbach array (Fig. 36) and cured in a 60°C oven. The purpose of the halbach array is to provide a homogenous magnetic field that aligns the particles in one orientation and prevents clustering. The homogeneity of the field also prevents the particles from drifting in any direction.

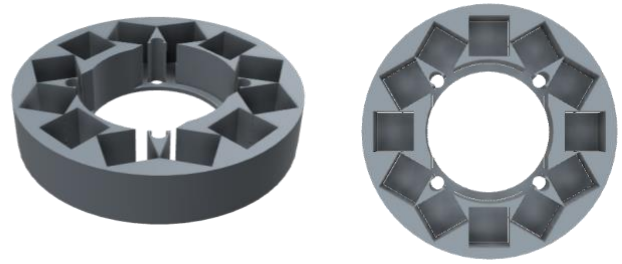


Fig. 36. CAD of halbach array container for magnets. A halbach array is used to create a homogenous magnetic field to prevent the magnetic particles from clustering or drifting.



Fig. 37. Assembled halbach array used to create a homogenous magnetic field to prevent the magnetic particle from clustering or drifting.

Two samples are fabricated; once they are cured they are magnetized using an ASC SCIENTIFIC Impulse Magnetizer (Model IM-10-30). Each sample is subject to 3 pulse at about 2.2 T. They are then characterized using a F.W BELL 5180 Gauss/Tesla meter as shown in Fig. 39. The characterization data and analysis is included in TABLE X. in the measurements section.



Fig. 38. ASC SCIENTIFIC impulse magnetizer (Model IM-10-30)



Fig. 39. F.W BELL 5180 Gauss/Tesla meter being used to characterize a fabricated magnetic sample made out of strontium ferrite and Ecoflex 30

If AlNiCo and NdFeB particles had been acquired then the same procedure would have been repeated to make the appropriate flexible bar magnets.

Singular integrated bar fabrication methodology: This method was not pursued due to constraints imposed by the COVID-19 pandemic, but it is included here as a potential fabrication method. This procedure involves first mixing the AlNiCo and NdFeB particles with Ecoflex 30 at different increasing volume ratios. The composition is then mixed in a Thinky mixer at 2000rpm for 30 seconds and allowed to cure in a halbach array placed in a 60°C oven. After curing it is also magnetized with a pulse magnetizer and characterized using a Gauss meter.

Rigid bar prototype: This method was also not pursued due to constraints imposed by the COVID-19 pandemic, but it is included here as a potential fabrication method. As the name suggests, this prototype consist of rigid bars. Therefore, these would not contribute to the total compliance of the device, but they have the advantage of being smaller and exerting greater force compared to a fabricated flexible magnet of equivalent size.

VI. EVALUATION/ VERIFICATION

A. Soft Iron Ends Measurements and Verification

This section discusses the technical specifications met by the soft iron ends prototype. Of the particles used to fabricate the ferroelastomers, the 100-micron ones exhibit the highest permeabilities across the range of volume ratios. These results were used to guide the fabrication of the particles in a shell samples; the 100-micron particles are embedded inside the particle in a shell samples.

Ferroelastomer prototype characterization: Characterization is done by connecting an RLC meter to a coil of 10mm diameter

and 200 turns. Each sample is inserted into this coil and the inductance measured. The values are recorded and can be found in appendix IX and X. Fig. 40 and Fig. 41 shows the inductance and permeability of the samples as a function of volume respectively.

Graph of Inductance at 1KHz in uH for Ecoflex 30
Each line represents particles of different sizes

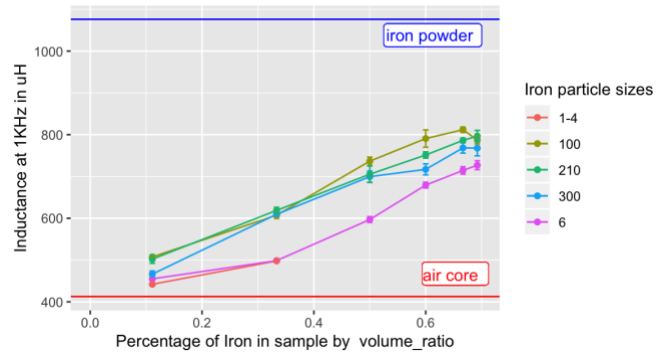


Fig. 40. Effect of increasing the percentage of iron on the inductance of the sample. The volume ratio refers to absolute volume ratio of iron. The blue line at the very top corresponds to the values of a shell filled with just iron filings. The red line at the bottom corresponds to the values of the coil with no core (ie. air core). Error bars are derived from the standard deviation.

Graph of Relative Permeability for Ecoflex 30
Each line represents particles of different sizes

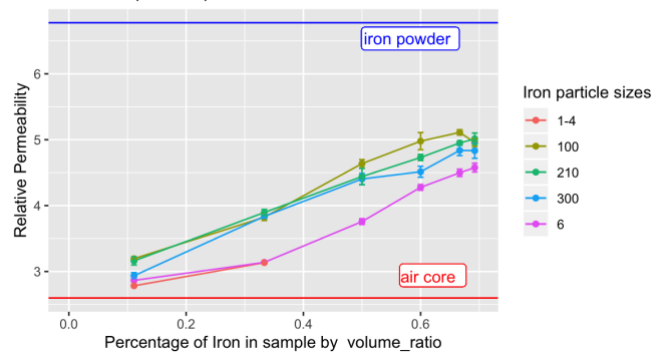


Fig. 41. Effect of increasing the percentage of iron on the inductance of the sample. The volume ratio refers to absolute volume ratio of iron. The blue line at the very top corresponds to the values of a shell filled with just iron filings. The red line at the bottom corresponds to the values of the coil with no core (ie. air core). Error bars are derived from the standard deviation.

As expected the values of inductance and permeability increase with increase in the percentage of iron. 100-micron particles exhibit the highest values of permeability for most of the volume ratios. However, the line has a dip after 0.66 volume ratio; at 0.69 the permeability seems to be lower than at 0.66. A similar trend is observed for the 300-micron particles where the permeability flattens out after 0.66 volume ratio. The reason for the flattening and dipping is still not know. This mystery however does not affect the choice of samples to use for the soft iron ends because the high volume-ratio samples have low compliance.

The same data used to make the volume ratio graphs is also used in Fig. 42 and Fig. 43 to create plots of inductance and permeability against mass ratio. The misalignment of the ratio values of the graph is due to the methodology of the experiment which prioritizes volume ratio alignment over mass ratio alignment. Regardless the graphs exhibit a similar general trend to that of the volume ratio where the inductance and permeability increases with increase in the ratio of iron.

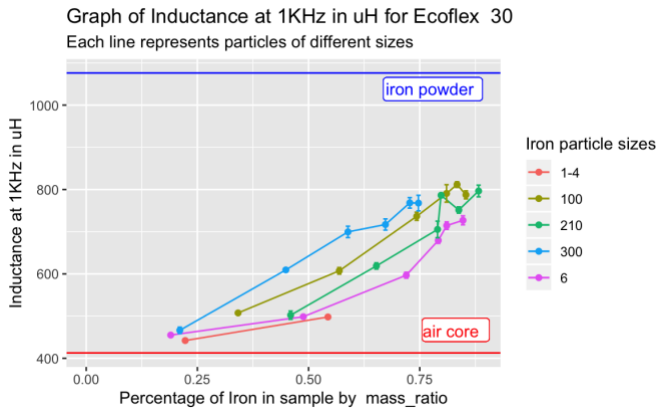


Fig. 42. Effect of increasing the percentage of iron by mass on the inductance. The mass ratio refers to absolute mass ratio of iron. Error bars are derived from the standard deviation.

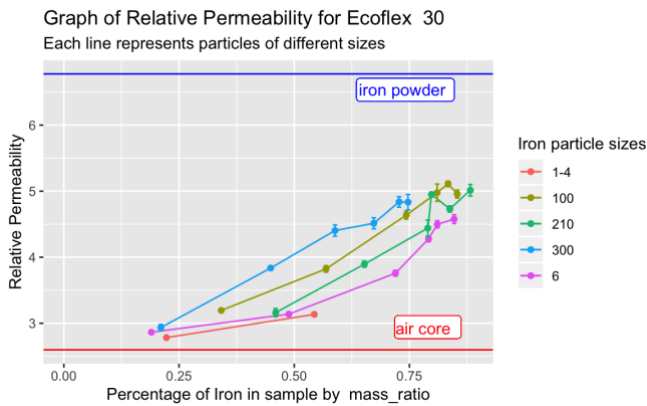


Fig. 43. Effect of increasing the percentage of iron by mass on the relative permeability. The mass ratio refers to absolute mass ratio of iron. Error bars are derived from the standard deviation.

The 1-4 micron particles have less data points on the plot because at higher ratios the mixtures failed to cure.

Some of the ferroelastomer samples are placed in a vacuum chamber before being placed in the oven. It is observed that the permeability of the vacuumed samples is generally lower than that of the non-vacuumed samples as shown in the figure below:

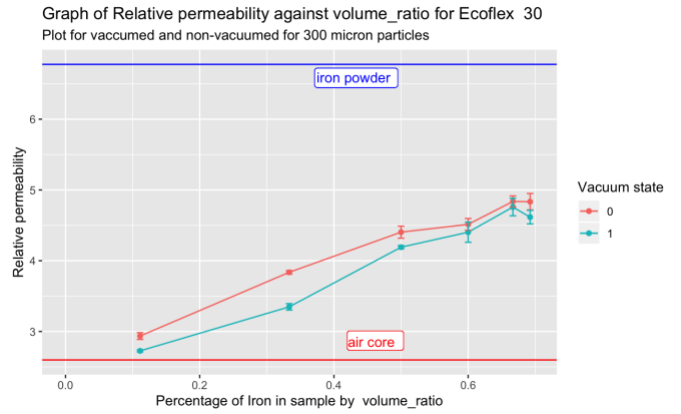


Fig. 44. Effect of vacuuming samples on the relative permeability of 300-micron particle samples. Plotted against absolute volume ratio of particles.

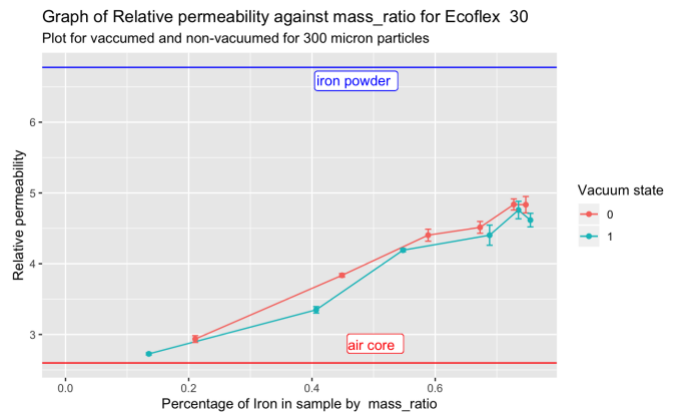


Fig. 45. Effect of vacuuming samples on the relative permeability of 300-micron particle samples. Plotted against absolute mass ratio of particles.

Particles in a shell characterization: While fabricating the shells, some samples are placed in a vacuum chamber to evict air pockets from the shell while others are not. The non-vacuumed samples exhibit higher permeability than the vacuumed samples as shown in TABLE V.

TABLE V. MEASURED INDUCTUANCE OF VACUMED AND NON-VACUMED PARTICLE IN A SHELL SAMPLES

Particles sizes (microns)	Vacuumed?	Mean Inductance	Standard Deviation of Inductance
100	Yes	690.65	23.47
100	No	791.02	18.39

Also, it was observed that particle in a shell samples have comparable permeability to the ferroelastomer samples with the highest absolute volume ratio (0.69). However, the particle in a shell sample offered higher compliance therefore would be more suitable for use in the assembly of the EPM actuator. This is summarized in the table below:

TABLE VI. COMPARISON OF INDUCTANCE OF NON-VACUUMED FERROELASTOMER AND NON-VACUUMED PARTICLE IN A SHELL SAMPLE

Sample type	Particles sizes (microns)	Mean Inductance	Standard Deviation of Inductance
Ferroelastomer	100	793.98	17.849
Particles in a shell	100	791.02	18.39

The achieved relative permeability value is 5.2. Literature does not dictate the value of permeability beyond which flux begins to stray therefore this would be determined empirically after assembling the device.

Compliance characteristics: Compliance characterization is done with an Instron device. Compression tests are conducted on two ferroelastomer samples and one particle in a shell sample. The Instron conducts a compression test by exerting a compressional force and measuring the change in length. Fig. 46 shows one such plot of force against time and extension against time for ferroelastomer sample 10. All the other samples exhibited a similar trend. Data from the compression tests is used to compute the Young's modulus of the samples as per Equation 6.

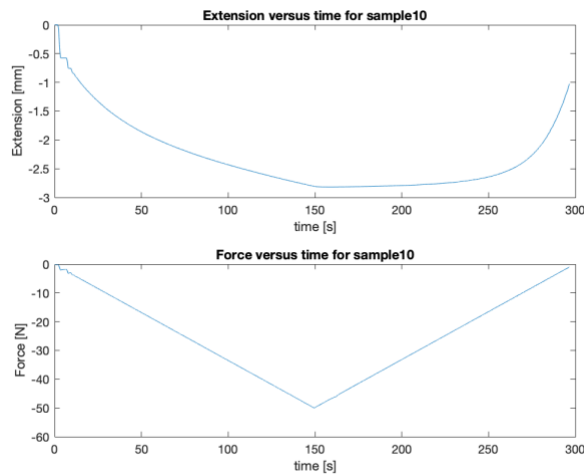


Fig. 46. Raw data plot of force against time and extension time for ferroelastomer sample 10

TABLE VII. summarized the compliance characteristics of the ferroelastomer samples and the particle in a shell sample. In the GPa scale the compliance rounds off to a value of 0.001 GPa, however there is a difference in compliance between the three different samples as shown in boxplot in Fig. 47 with the particle in a shell sample exhibiting the highest compliance.

TABLE VII. COMPLIANCE CHARACTERISTICS

Sample type	Particles sizes (microns)	Mean Inductance (uH)	Mean Compliance (GPa)
Ferroelastomer, Sample #10	100	790.72	0.001
Ferroelastomer, Sample #11	100	811.84	0.001
Particle in a shell, mesh 20 particles	100	791.02	0.001

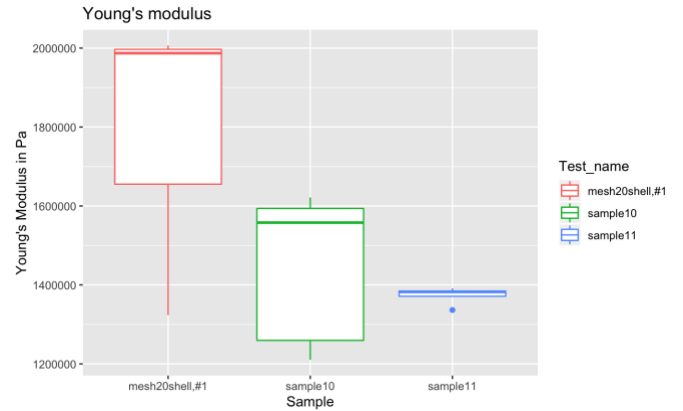


Fig. 47. Box plot of the compliance of two ferroelastomer samples (sample 10 and sample 11) and one particle in a shell sample (mesh20shell#1). The middle line indicates the median of the measurements.

B. Soft Coil Measurements and Verification

In the fabrication of the coils, the first three prototypes lost their ability to conduct after being wound on the mold. The loss in conductivity is due to separation in the liquid metal alloy channel as a result of being stretched. However, before they lost their ability to conduct, the resistance was measured, and their electrical characteristics used to derive the conductivity of EGaIn as shown in TABLE VIII. below. The average resistivity is $2.48 \times 10^{-7} \Omega m$ with a standard deviation of $4.7043 \times 10^{-8} \Omega m$. Resistivity is the reciprocal of conductivity: $\sigma = 4.03 \times 10^6 Sm^{-1}$.

TABLE VIII. SOFT WIRE CHARACTERIZATION

Tube diameter (mm)	EGaIn Length (m)	Electrode diameter	Electrode length (m)	Total Resistance (Ω)	Computed EGaIn resistivity (Ωm)
0.3	1.20	30 AWG (0.254 mm)	0.11	3.566	2.0791E-7
0.3	1.705	28 AWG (0.32004 mm)	0.14	5.74	2.368E-7
0.5	4	22 AWG (0.64516 mm)	0.073	6.115	2.999E-7

The fourth prototype successfully retained its conductivity because it was first wound on the mold with less turns and less stress before injecting EGaln into the tube. The results are shown in TABLE IX. Conclusively, it is recommended to wind first before injecting EGaln in the fabrication of the coil:

TABLE IX. PROTOTYPE IV COIL CHARACTERISTICS

Tube diameter (mm)	EGalN Length (m)	Electrode diameter	Electrode length (m)	Total R (Ω)	EGalN resistivity (Ωm)	N	L μH
0.3	0.409	28 AWG (0.32004 mm)	0.17	1.413	2.38E-7	10	1.67

The values in TABLE IX. are used to make a series RLC model consisting of the coil and a $400\mu F$ capacitor charged to 30 V. These values result in an overdamped RLC circuit hence Equation 16 (equation for the overdamped RLC circuit) is used to determine the maximum current. Fig. 48 show the transient current plot for the prototype IV coil.

$$\omega_0 = \sqrt{\left(\frac{R}{2L}\right)^2 - \frac{1}{LC}}$$

$$i(t) = \frac{V_0}{\omega_0 L} e^{-\frac{Rt}{2L}} \sinh \omega_0 t$$

Equation 16

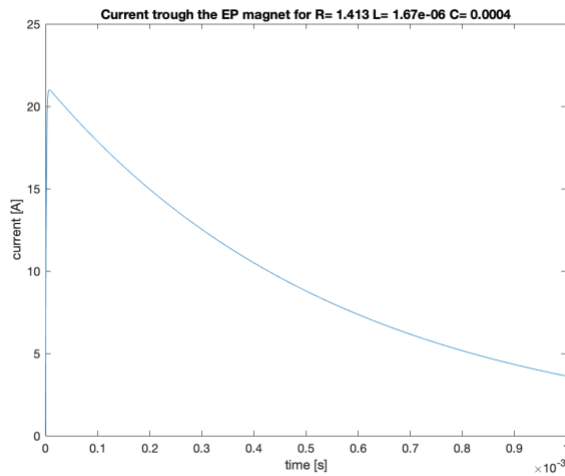


Fig. 48. Plot of current against time for prototype IV coil.

The maximum current is observed to be about 21 A. While this is a high value, the quantity that matters in the design of the coil is the magnetic field strength. Fig. 49 shows the potential for optimization that could be done on the coil to further increase the current as well as the impact of varying number of turns and

the diameter of the tube. To compute the resistance and inductance of the coil the equation below are used.

$$R = \frac{\rho \ell_{tube}}{A_{tube}}$$

$$L = \frac{\mu N^2 A_{coil}}{\ell_{coil}}$$

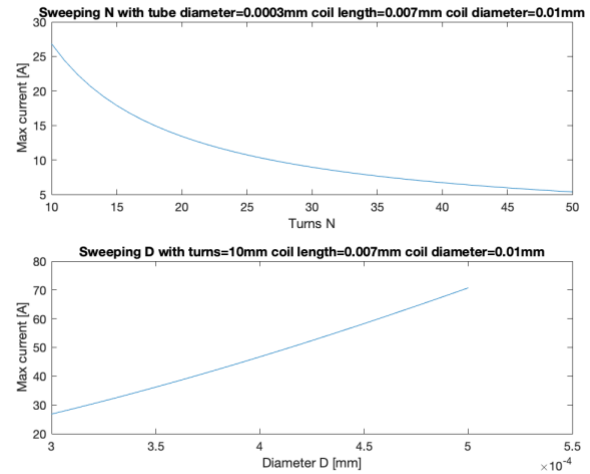


Fig. 49. Sweeping number of turns and tube diameter while computing the maximum current.

Magnetic field strength characterization: The original plan was to empirically measure the magnetic flux density using the F.W BELL 5180 Gauss/Tesla meter. The setup would have involved connecting the coil to a current source and placing a gauss meter probe inside the coil to measure the flux (B). The field strength(H) would then be calculated from the magnetic flux(B). This however could not be done due to time constraints and resource constraints imposed by the COVID-19 pandemic; therefore, an estimation of the coil's magnetic field strength was done through simulation by applying Equation 17. The simulation achieved a H value of 25 kA/m.

$$H_{coil} = \frac{N I_{coil}}{\ell_{coil}}$$

Equation 17

A simulation is also done to iterate over different number of turns and different tube diameters to optimize the magnetic field strength. It reveals the trend shown in Fig. 50.

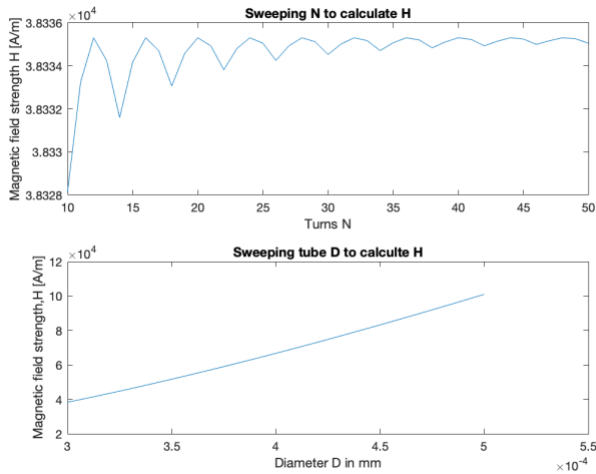


Fig. 50. Iterating over number of turns and tube diameter while computing the magnetic field strength(H).

Fig. 50 shows that with a tube of 0.5mm inner diameter, 10 turns and coil length of 0.7 mm then the target magnetic field strength of 100 kA/m can be achieved.

Transient current limit: Literature does not point to the amount of transient current that would cause an EGaIn conductor to undergo a change in its ability to conduct. Regardless this can be determined empirically by taking a short EGaIn tube conductor of, for example, 100 mm length and sequentially passing a predetermined amount of current. A short conductor is necessary here so as to have an equivalently lower resistance and achieve higher transient currents. The transient current is driven through the wire for about 50 μ s then and the resistance measured. The objective is to determine whether high currents alter the resistance. An increase in resistance would indicate damage to the wire due to heat dissipation from I^2R losses. This experiment was also not conducted due to the pandemic.

C. Magnetic Core Measurement and Verification

The ideal material for fabricating the semi-hard and hard permanent magnets are AlNiCo LNG40 and NdFeB N40. These could not be acquired; therefore, strontium ferrite was used in the place to prove the feasibility of the fabrication processes developed herein.

Remanence: TABLE X. summarizes the remanence of the fabricated strontium ferrite samples. The samples have cylindrical shape with a top smooth surface and a bottom rough surface. The “edge” refers to the curved surface. The measurements were done by placing a probe against the different surfaces as illustrated previously in Fig. 39.

The results in TABLE X. show that the residual magnetism is significantly lower by three orders of magnitude compared to the desired value of about 1.27 T of NdFeB and AlNiCo.

Strontium ferrite therefore would not suit the EPM design, but the fabrication process can be replicated with NdFeB and AlNiCo powder for better results in future work.

TABLE X. STRONTIUM FERRITE MAGNETIC CHARACTERISTICS

Sample #	Mass ratio of SrFe	Smooth side [T]	Rough side [T]	Edge B [T]
1	0.8	0.015	0.006	0.026
2	0.7	0.015	0.006	0.014

Coercivity: Coercivity can be measured using a pulse magnetizer and a Gauss meter. The proposed procedure involved applying a magnetic field on each prototype at intervals of 0.3 T up to a maximum of 2.7 T. After each interval the residual magnetic field is measured. The coercivity of strontium ferrite could not be measured due to the closure of the laboratories.

Compliance: It is projected that the compliance of the permanent magnets would have resembled that of the ferroelastomer soft iron ends given the similarity of the fabrication process and the similar particulate nature of the raw materials.

D. Assembled Device Measurement and Verification

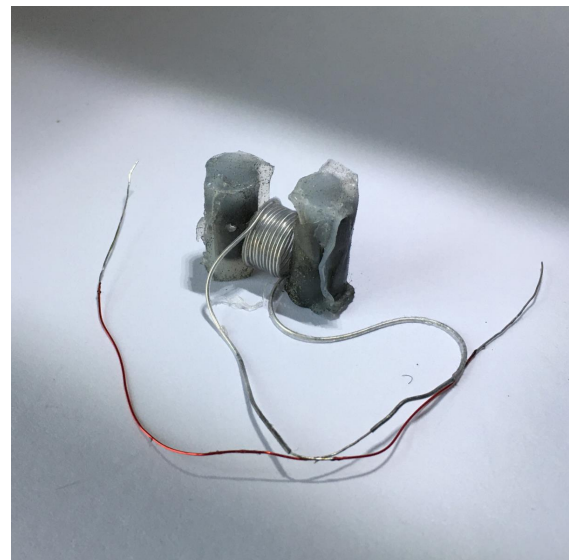


Fig. 51. Concept image of the assembled EPM. The particle in a shell soft iron ends are placed adjacent to the coil. There is no magnetic core in the center of the coil in this image.

Fig. 51 shows what the assembly would have looked like once completed. This image consists of just the soft iron ends and the coil. This arrangement is sufficient to measure some of the desired specifications (such as size) as discussed below.

Length: The assembly in Fig. 51 has a length of 2cm measured from soft end to soft end. This was close to the target of 1cm.

Holding Force: The holding force of the device could not be measured as the assembly was not completed. If completed, the holding force would have been measured by attaching the EPM to a target surface placed on a weighing scale. Pulling on the EPM until it detaches from the target surface would alter the reading on the weighing scale. The difference in the reading just before the EPM detaches and the reading when the EPM is not being pulled would correspond to the holding force.

Compliance: The overall compliance could not be measured because of the absence of the assembly. However, the individual components attained a compliance within the target range suggesting that the assembled device would have also had the similar compliance.

Actuation performance: The soft EPM would have been tested against a rigid EPM to determine its latching performance on different geometric surfaces. The proposed setup involves steel balls of different diameters and steel cubes of different dimensions. The EPMs would be latched onto the surfaces of each of the steel objects and the force needed to detach them measured using a string tied to a spring of known spring constant k .

VII. BUDGET

A complete list of the purchased materials used in this project is attached in appendix XI. The design and fabrication cost for this project estimated to be about \$1136. However, the cost of reproducing the components using the fabrication procedures provided here is projected to be significantly less. TABLE XI. summarizes the cost of reproducing a hypothetically functioning prototype without factoring in the tools, machinery and measuring instruments used to fabricate the components. The estimation is based on the materials listed in the budget in appendix XI.

TABLE XI. FABRIATION COST OF A SOFT EPM WITH MINIMUM MATERIALS NEEDED

Component	Estimated Reproduction Cost
Flexible soft iron ends	\$ 90
Flexible coil	\$ 140
Hard magnet using NdFeB	\$ 250
Semi-hard magnet using AlNiCo	\$ 200

VIII. CONCLUSION AND FUTURE WORK

A. Summary of Achieved Technical Specifications

TABLE XII. summarizes the achieved values with regards to the technical specifications. The dashed fields correspond to quantities that could not be measured due to the unanticipated

constraint imposed by the 2020 COVID-19 pandemic. However, procedures for quantifying the corresponding components is included in the prototyping and measurement sections:

TABLE XII. SUMMARY OF TECHNICAL SPECIFICATIONS

Specification	Target value	Achieved value
Device Scale	1 cm long	2.7 cm long
Holding Force	1.7 N	-
Soft Iron End relative permeability	10	5.2
Soft Iron End compliance	0.001 to 0.05 GPa	0.001 to 0.002 GPa
Hard Permanent Magnet coercivity	1000 kA/m	-
Semi-hard Permanent coercivity	50 kA/m	-
Semi-hard Permanent magnet compliance	0.001 to 0.05 GPa	0.001 to 0.002 GPa
Coil conductivity	$3.4 \times 10^6 Sm^{-1}$	$4.03 \times 10^6 Sm^{-1}$
Coil magnetic field strength	100 kA/m	25 kA/m
Coil transient current limit	20 A	-

B. Discussion

The objective of this project has been to design and fabricate soft composite materials that could be used in magnetic actuators. These composite materials have been used to attempt to convert a rigid EPM actuator into a compliant one with higher compatibility for soft robotics and higher surface adaptation characteristics. Such a device can be used in self assembling robotic systems by embedding them in joints or in robots that have to navigate over magnetic surfaces.

Furthermore, the composite materials developed here have immediate application in electromagnetic and magnetic actuators in need of higher compliance. The author suggests that the soft EPM components and materials developed herein can be adapted and tested on other magnetic and electromagnetic actuators such as relays, valves and motors.

The device size was not too far off from the target value; however, since the energy requirement of an EPM scales with the volume, then this achieved value would result in a higher power requirement than if the size was 1cm.

The target compliance was achieved for the fabricated components. The soft iron ends, coil and SrFe magnets all had a compliance within the 0.001 to 0.05 GPa range with a minimum of 0.001 GPa.

The conductivity of the fabricated EGaIn coil matched the literature value of within the same order of magnitude.

C. Future Work

It is still uncertain whether the permeability of the soft iron ends achieved here significantly impacts the functionality of the EPM; this would have to be determined empirically.

The fabrication processes for the semi-hard and hard permanent magnets were not fully explored, but proposed procedures and recommendations have been included for those who may be interested in building upon this work.

The coil achieved a magnetic field strength(H) of 25kA/m. However as shown in the measurements section, adjustments can be done on the number of turn and the size of the conductive tube's diameter to increase the magnetic field strength up to about 100kA/m.

The device size can further be miniaturized to leverage the energy to volume scaling relations of EPM so as to decrease the power requirements.

Given that most of the parts were fabricated out of Ecoflex the potential of adapting the device design geometries to suite custom robots is unbound; the composite materials can take almost any shape. An advanced version of this project would involve a sophisticated fabrication process with a custom 3D printer to dispense composite materials and extrude desired shapes directly into the structure of soft robotic systems. Even without a 3D printer custom molds can be used to embed EPMs directly into soft robotic systems. Specialized fabrication methods such as the latter and former would allow for the production of actuators at an even smaller scale which would leverage the EPMs energy efficiency because, as discussed in this report, the switching energy scales with the volume.

IX. ACKNOWLEDGMENT

The author gratefully acknowledges the contribution of Bahar Haghighat, Radhika Nagpal, Anas Chalah, Daniel Prendergast, the active leaning labs(ALL) staff, the ES100 staff and fellow ES100 peers for their guidance and support throughout this project. Their contributions were instrumental to the success of this project

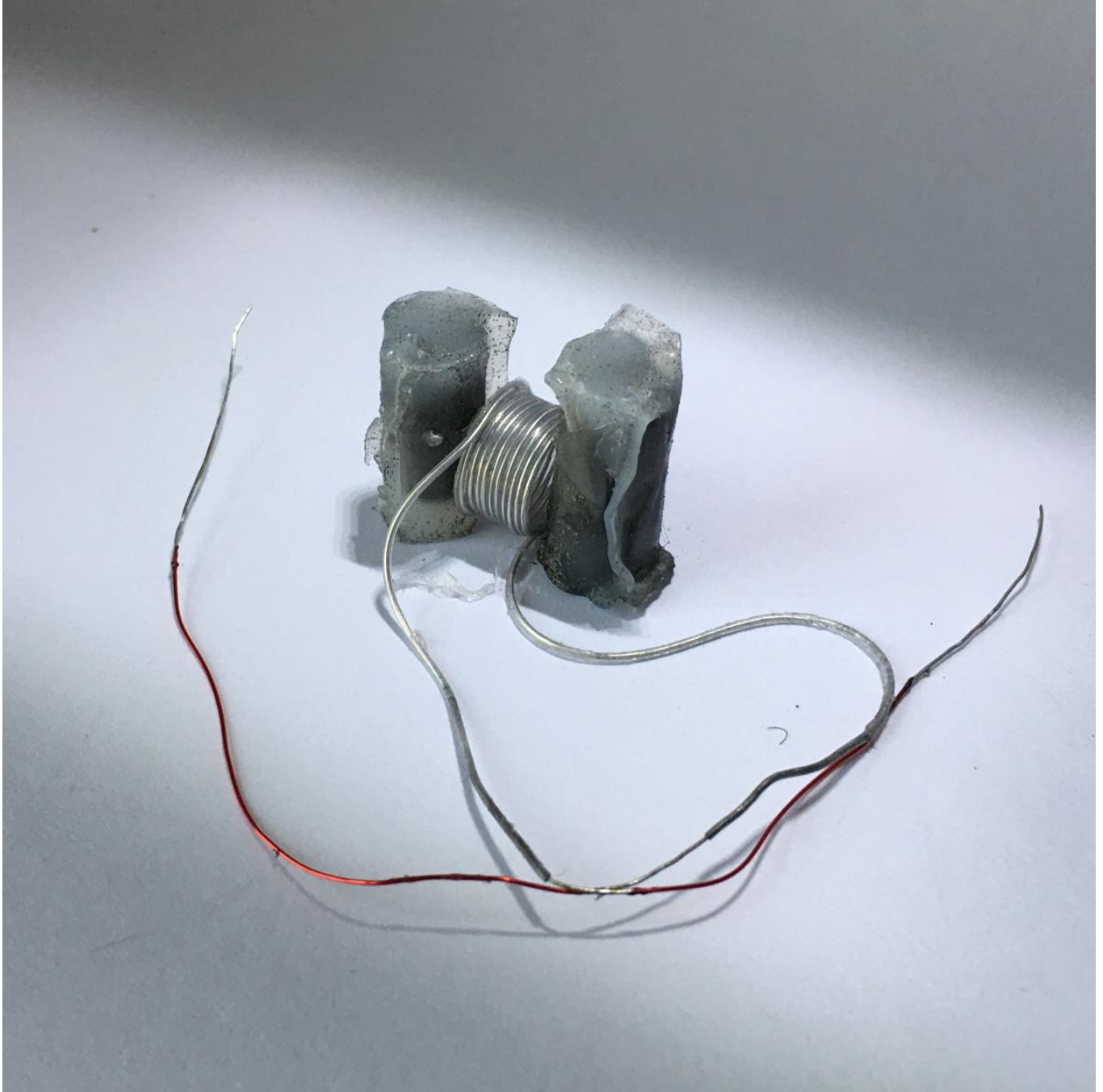
X. REFERENCES

- [1] F. Ilievski, A. D. Mazzeo, R. F. Shepherd, X. Chen, and G. M. Whitesides, "Soft Robotics for Chemists," *Angewandte Chemie International Edition*, vol. 50, no. 8, pp. 1890–1895, 2011, doi: 10.1002/anie.201006464.
- [2] "Challenges and Opportunities for Design, Simulation, and Fabrication of Soft Robots | Soft Robotics." <https://www.liebertpub.com/doi/abs/10.1089/soro.2013.0007> (accessed Oct. 02, 2019).
- [3] P. Boyraz, G. Runge, and A. Raatz, "An Overview of Novel Actuators for Soft Robotics," *Actuators*, vol. 7, no. 3, p. 48, Sep. 2018, doi: 10.3390/act7030048.
- [4] A. N. (Ara N. Knaian, "Electropermanent magnetic connectors and actuators : devices and their application in programmable matter," Thesis, Massachusetts Institute of Technology, 2010.
- [5] R. Guo, L. Sheng, H. Gong, and J. Liu, "Liquid metal spiral coil enabled soft electromagnetic actuator," *Sci. China Technol. Sci.*, vol. 61, no. 4, pp. 516–521, Apr. 2018, doi: 10.1007/s11431-017-9063-2.
- [6] J. F. Shackelford, *Introduction to materials science for engineers*, Eighth edition. Boston: Pearson, 2015.
- [7] S. Tumański, *Handbook of Magnetic Measurements*. 2016.
- [8] "Ferrimagnetism | physics," *Encyclopedia Britannica*. <https://www.britannica.com/science/ferrimagnetism> (accessed Apr. 07, 2020).
- [9] M. Raad, "Miniature Electro-Permanent Magnets for Modular Soft Robots." .
- [10] B. Haghighat, E. Droz, and A. Martinoli, "Lily: A miniature floating robotic platform for programmable stochastic self-assembly," in *2015 IEEE International Conference on Robotics and Automation (ICRA)*, May 2015, pp. 1941–1948, doi: 10.1109/ICRA.2015.7139452.
- [11] "Miniature Soft Electromagnetic Actuators for Robotic Applications - Do - 2018 - Advanced Functional Materials - Wiley Online Library." <https://onlinelibrary.wiley.com/doi/abs/10.1002/adfm.201800244> (accessed Oct. 04, 2019).
- [12] "Micrometals Powder Core Solutions." <https://micrometals.com/materials/pc> (accessed Mar. 01, 2020).
- [13] "MAGNETISM.eu - EMA - The European Magnetism Association." <http://magnetism.eu/> (accessed Oct. 04, 2019).
- [14] "Physics - Young's modulus - University of Birmingham." <https://www.birmingham.ac.uk/undergraduate/preparing-for-university/stem/Physics/stem-legacy-Youngs-modulus.aspx> (accessed Oct. 06, 2019).
- [15] G. Bai, R. W. Gao, Y. Sun, G. B. Han, and B. Wang, "Study of high-coercivity sintered NdFeB magnets," *Journal of Magnetism and Magnetic Materials*, vol. 308, no. 1, pp. 20–23, Jan. 2007, doi: 10.1016/j.jmmm.2006.04.029.
- [16] P. Campbell and S. Al-Murshid, "A model of anisotropic Alnico magnets for field computation," *IEEE Transactions on Magnetics*, vol. 18, no. 3, pp. 898–904, May 1982, doi: 10.1109/TMAG.1982.1061943.
- [17] G. J. Hayes, Ju-Hee So, A. Qusba, M. D. Dickey, and G. Lazzi, "Flexible Liquid Metal Alloy (EGaIn) Microstrip Patch Antenna," *IEEE Trans. Antennas Propagat.*, vol. 60, no. 5, pp. 2151–2156, May 2012, doi: 10.1109/TAP.2012.2189698.
- [18] "GitHub - kimkoech/ferroelastomer_property_analysis: Analysis of the permeability and compliance of different mixtures of iron and elastomers." https://github.com/kimkoech/ferroelastomer_property_analysis (accessed Mar. 01, 2020).

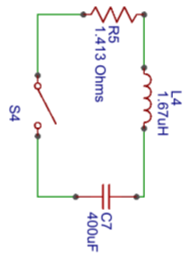
APPENDICES – DRAWING PACKAGE


XI. APPENDICES

APPENDIX I – CONCEPT IMAGE OF THE SOFT EPM ASSEMBLY

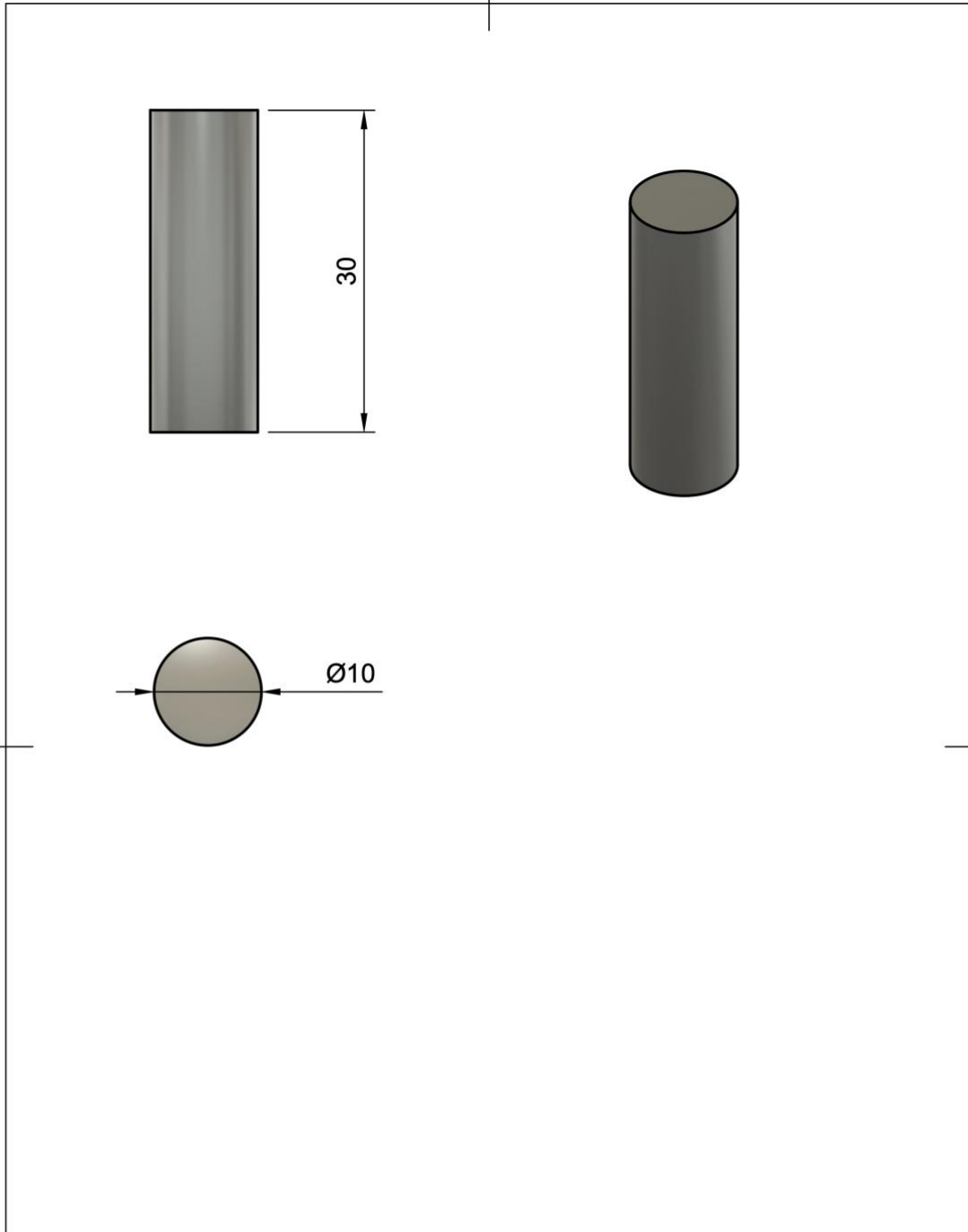


APPENDIX II – RLC MODEL OF PROTOTYPE IV COIL WITH A 400μF CAPACITOR



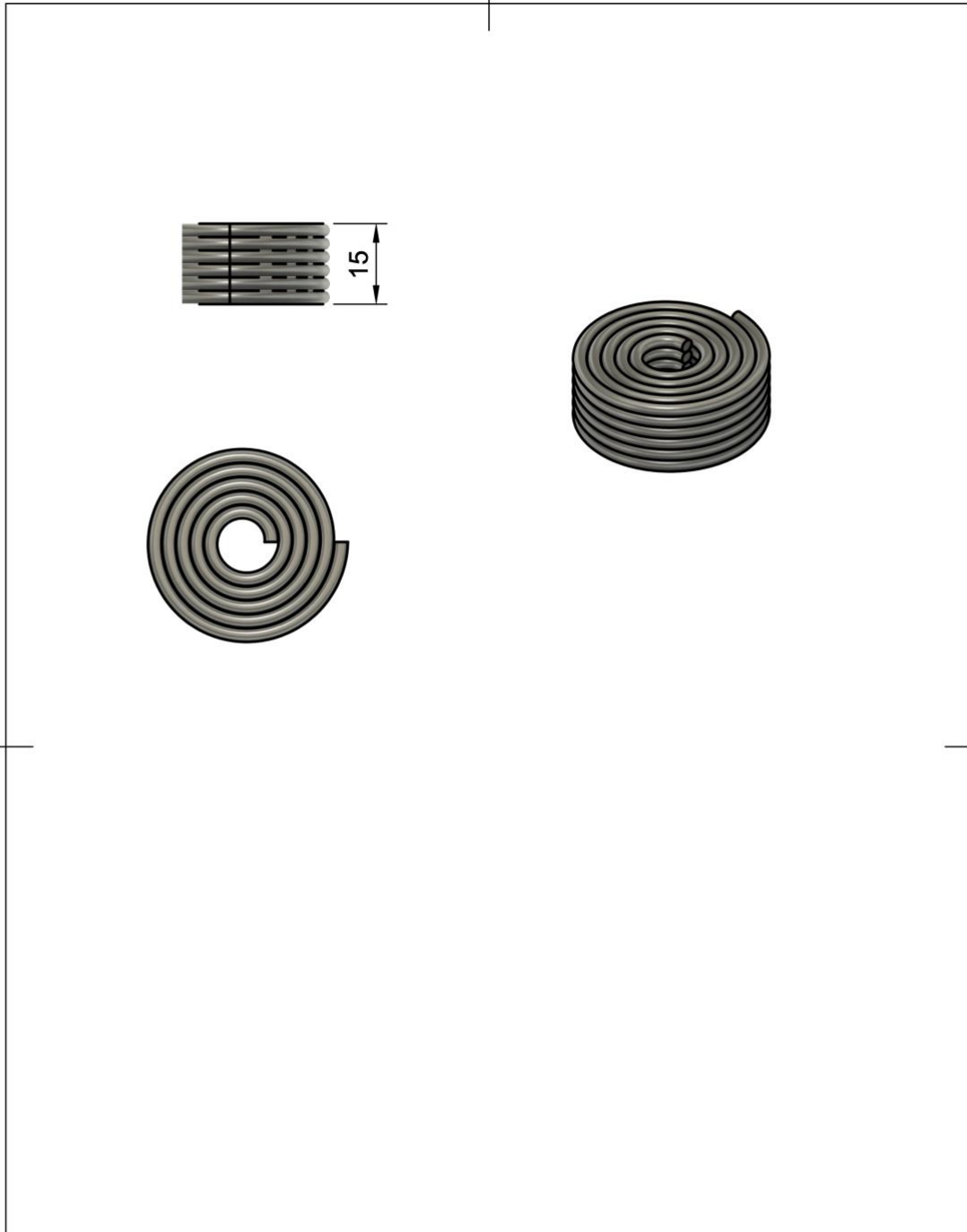
		TITLE: RLC Model of Soft EPM coil using Prototype IV	REV: 1.0
Company: Harvard SEAS		Sheet: 1/1	
Date: 2020-03-29		Drawn By: Billy Koech	

APPENDIX III – GEOMETRY OF THE PARTICLE IN A SHELL MODEL



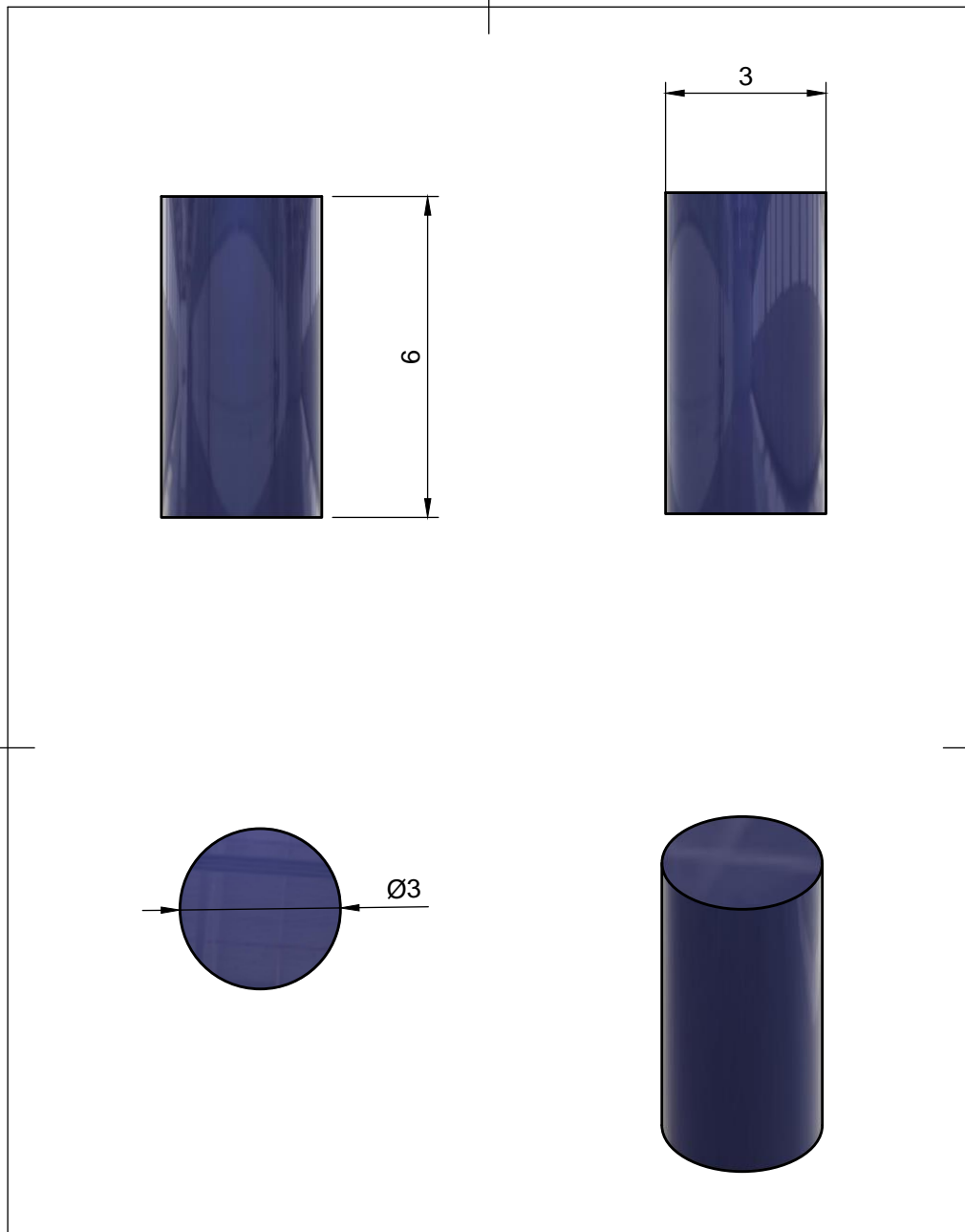
Dept.	Technical reference	Created by Billy Koech	4/9/20		Approved by
		Document type	Document status		
		Title particle in a shell geometry	DWG No.		
		Rev.	Date of issue	Sheet 1/1	

APPENDIX IV – CAD MODEL OF THE COIL



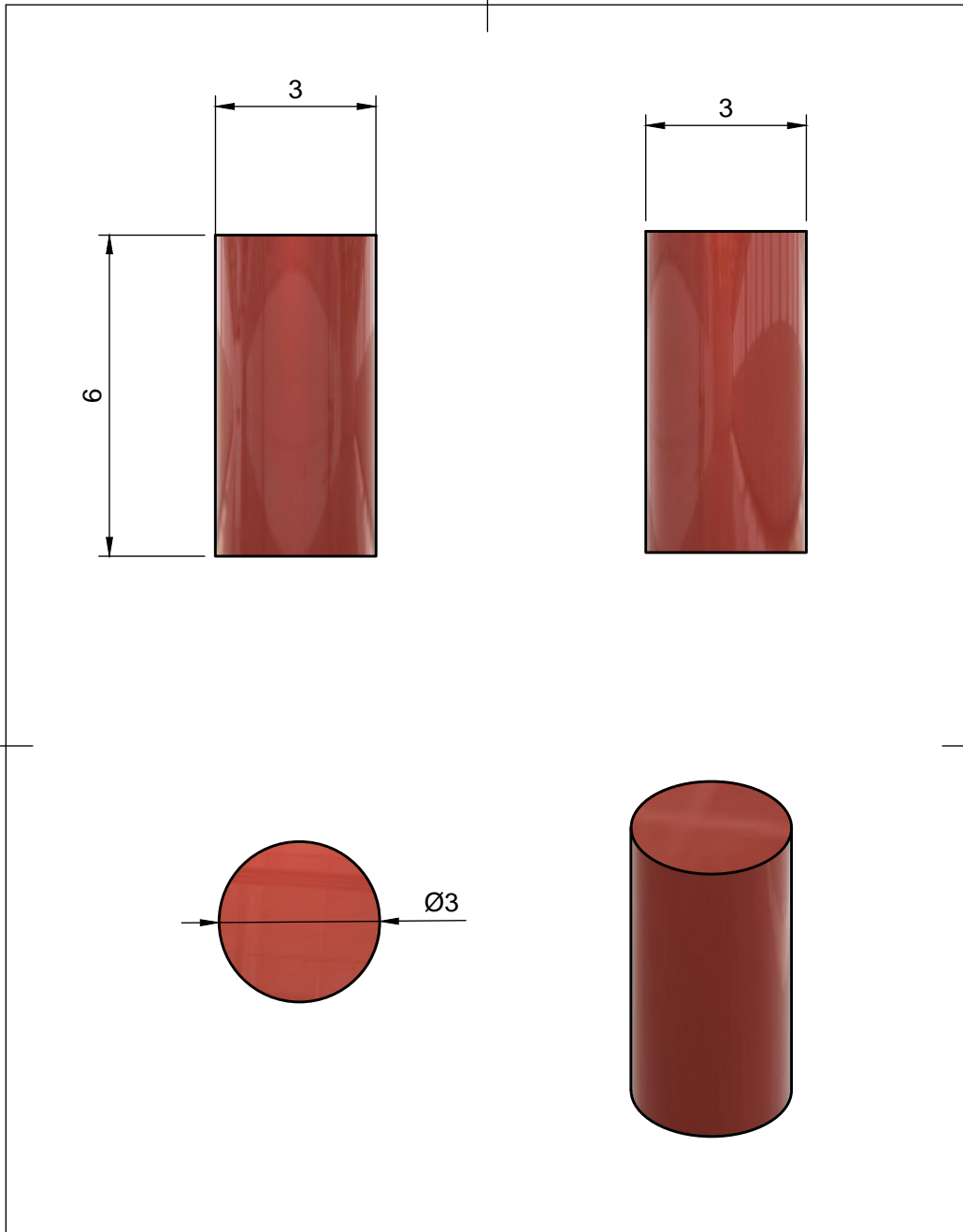
Dept.	Technical reference	Created by Billy Koech	4/9/20		Approved by
		Document type	Document status		
		Title coil	DWG No.		
		Rev.	Date of issue	Sheet 1/1	

APPENDIX V – FLEXIBLE SEMI HARD PERMANENT MAGNET GEOMETRY



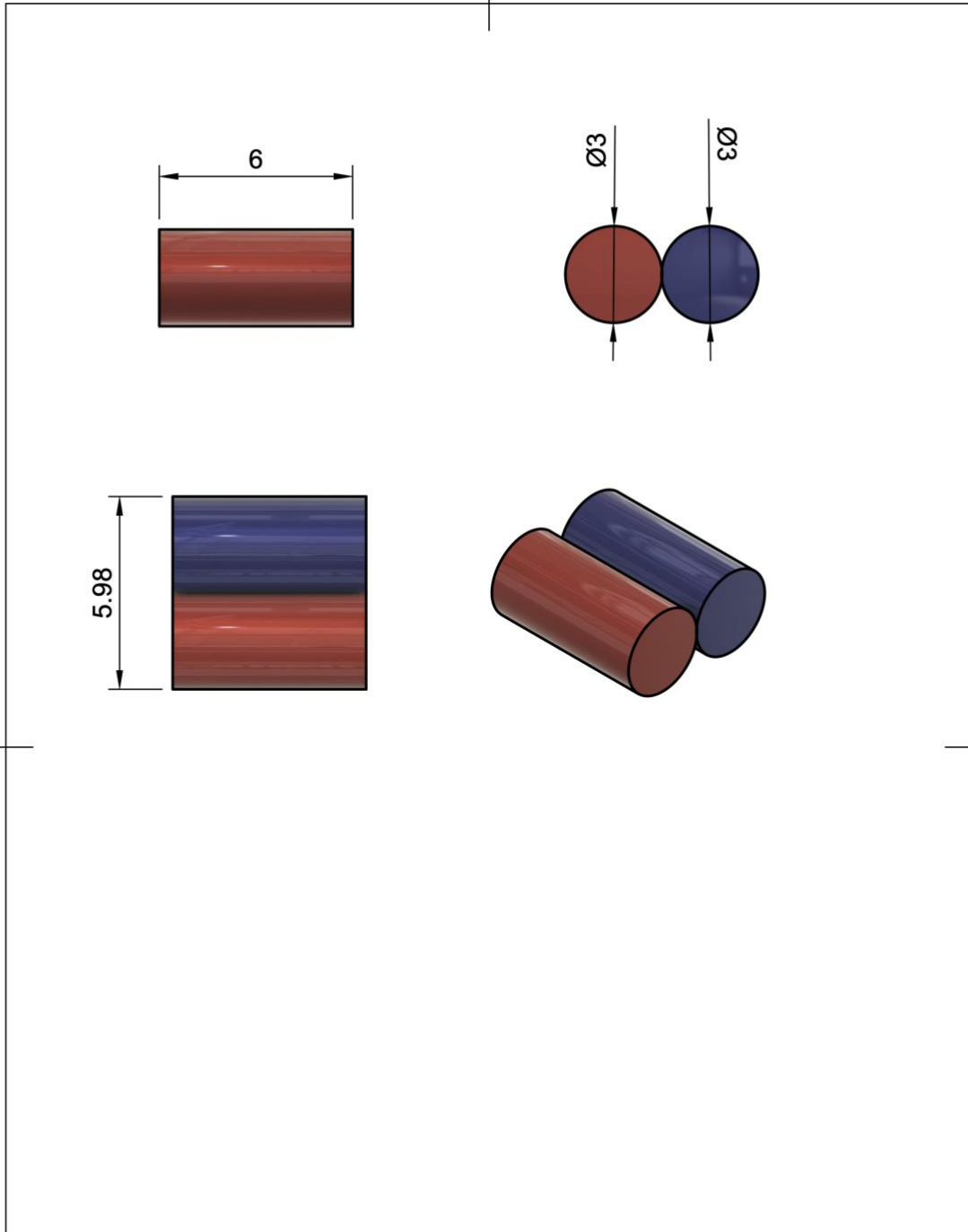
Dept.	Technical reference	Created by Billy Koech	11/6/19	Approved by	
		Document type	Document status		
		Title Semi-Hard Permanent Magnet	DWG No.		
		Rev.	Date of issue	Sheet	1/1

APPENDIX VI – FLEXIBLE HARD PERMANENT MAGNET GEOMETRY



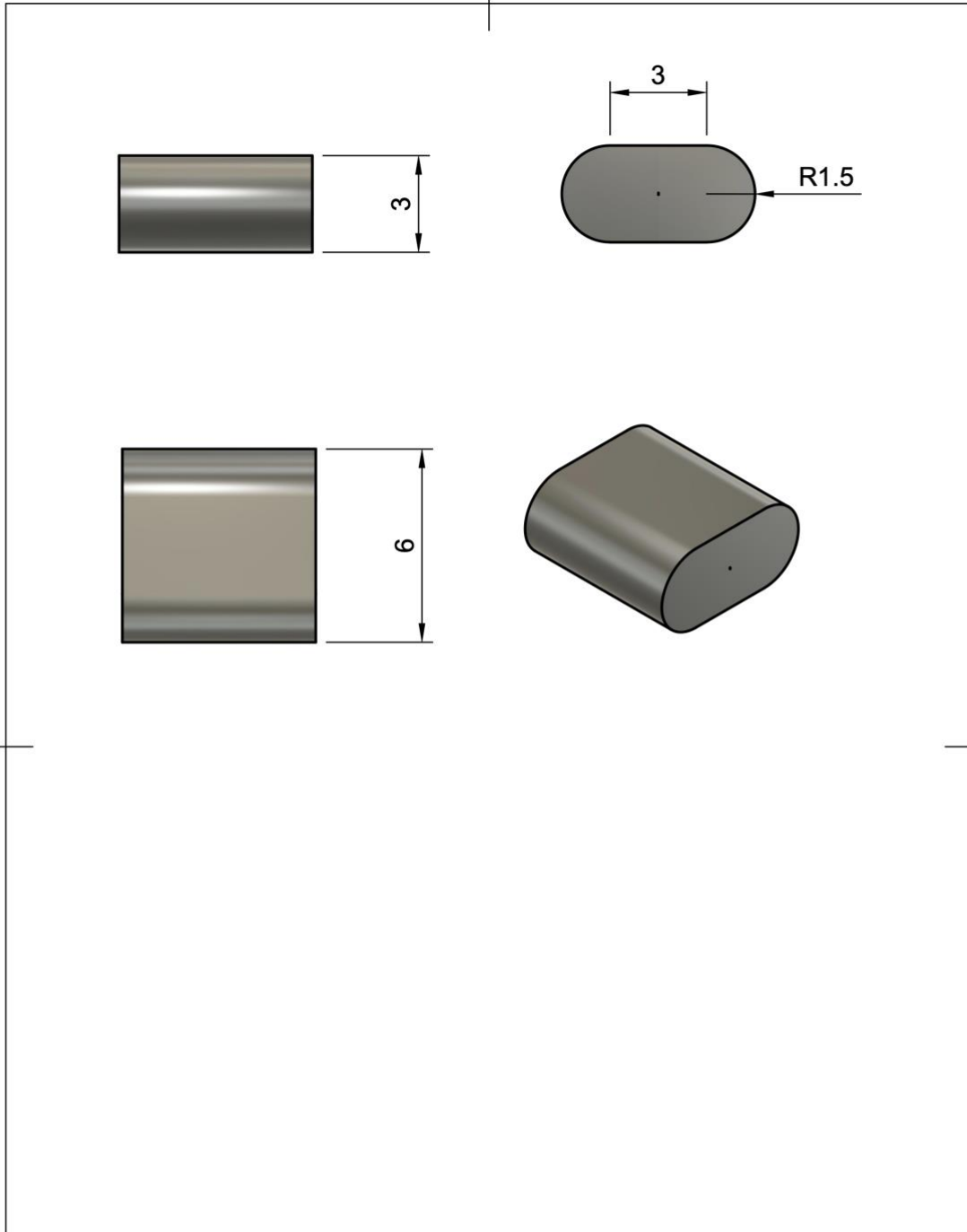
Dept.	Technical reference	Created by Billy Koech	11/6/19	Approved by
		Document type	Document status	
		Title Hard Permanent Magnet	DWG No.	
		Rev.	Date of issue	Sheet 1/1

APPENDIX VII – NdFeB AND AlNiCo ADJACENT TO EACH OTHER (SEPARATE BAR PROTOTYPE)



Dept.	Technical reference	Created by Billy Koech	Approved by 4/9/20
		Document type	Document status
		Title NdFeB and AlNiCo Adjacent to each other	
		Rev.	Date of issue

APPENDIX VIII – COMBINED AlNiCo and NdFeB (SINGULAR INTERGRATED BAR PROTOTYPE)



Dept.	Technical reference	Created by Billy Koech	4/9/20		Approved by
		Document type		Document status	
		Title Combined NdFeB and AlNiCo		DWG No.	
		Rev.	Date of issue	Sheet 1/1	

APPENDIX IX – INDUCTANCE OF SAMPLES FABRICATED WITH ECOFLEX 30

<i>Sample number</i>	<i>Volume Ratio</i>	<i>Particle size in microns</i>	<i>Mass ratio</i>	<i>Ecoflex type</i>	<i>Vacuumed?</i>	<i>Average inductance in uH</i>	<i>Standard deviation of inductance</i>	<i>Median inductance in uH</i>
1	0.09615385	210	0.25696594	30	0	443	5.90550591	442.9
2	0.27272727	210	0.57803762	30	0	529.02	34.4605862	525.9
3	0.38461538	210	0.68006008	30	0	590.32	21.9175044	580.7
4	0.5	210	0.77412399	30	0	689.74	4.66936827	686.9
5	0.6	210	0.84102268	30	0	786.38	20.4585434	790.1
6	0.63636364	210	0.86850153	30	0	845.1	12.6200238	844.4
7	0.11111111	100	0.27868852	30	0	461.24	2.12202733	460
8	0.33333333	100	0.56903353	30	0	607.3	7.80224327	606.9
9	0.5	100	0.74321985	30	0	736.6	9.68090905	734.2
10	0.6	100	0.81024989	30	0	790.72	20.7183976	782.6
11	0.66666667	100	0.83388218	30	0	811.84	6.50676571	812.5
12	0.69230769	100	0.8538961	30	0	793.98	17.849986	790
13	0.11111111	300	0.21052632	30	0	466.34	7.58142467	465.6
14	0.33333333	300	0.44880952	30	0	609.4	3.89679355	610.1
15	0.5	300	0.58854626	30	0	699.54	13.4988148	703.2
16	0.6	300	0.67280453	30	0	717.02	13.2861582	723.4
17	0.66666667	300	0.72754313	30	0	768.4	12.4925978	761.6
18	0.69230769	300	0.74704619	30	0	767.88	18.4552702	763.2
19	0.5	300	0.56962025	30	2	629.16	6.01564627	627.1
20	0.11111111	6	0.19	30	0	455.02	0.94180677	454.9
21	0.33333333	6	0.48813559	30	0	498.56	1.44499135	498.5
22	0.5	6	0.71965318	30	0	596.86	7.01305925	600.2
23	0.6	6	0.79161028	30	0	679.32	6.98333731	683.4
24	0.66666667	6	0.81055156	30	0	714.46	8.8429633	718.7
25	0.69230769	6	0.84712111	30	0	727	10.6400188	734.2
26	0.11111111	1-4	0.22259136	30	0	442.04	0.62289646	441.8
27	0.33333333	1-4	0.54356061	30	0	497.94	1.225969	498
32	0.11111111	100	0.34146341	30	0	507.44	0.68774995	507.6
33	0.69230769	100	0.85378835	30	0	787.42	9.5470938	788.3
34	0.11111111	210	0.3615495	20	0	482.68	3.22753776	482.7
35	0.33333333	210	0.65570008	20	0	633.5	0.86890736	633.4
40	0.11111111	210	0.4596577	30	0	502.18	9.93614613	502.5
41	0.33333333	210	0.65245374	30	0	618.82	7.47810136	620.1
42	0.5	210	0.78998073	30	0	705.38	19.6643586	703.6
43	0.6	210	0.83777068	30	0	751.38	7.43283257	754.5
44	0.66666667	210	0.79794118	30	0	786.38	5.30678811	784.8

APPENDIX IX – INDUCTANCE OF SAMPLES FABRICATED WITH ECOFLEX 30

45	0.69230769	210	0.88229084	30	0	796.48	13.8591847	801.2
47	0.11111111	300	0.1352459	30	1	433.06	2.47749874	433
48	0.33333333	300	0.40684932	30	1	531.88	7.24548135	532.7
49	0.5	300	0.54771784	30	1	665.76	3.66851469	664.8
50	0.6	300	0.68828298	30	1	699.42	22.6114352	700.1
51	0.66666667	300	0.73511543	30	1	755.88	19.6403157	756.5
52	0.69230769	300	0.75447427	30	1	733.28	15.3002288	730.6

APPENDIX X – RELATIVE PERMEABILITY OF SAMPLES FABRICATED USING ECOFLEX 30

<i>Sample Number</i>	<i>Volume ratio</i>	<i>Particle size</i>	<i>Mass ratio</i>	<i>Ecoflex type</i>	<i>Vacuumed?</i>	<i>Average relative Permeability</i>	<i>Standard Deviation of relative permeability</i>	<i>Median of relative permeability</i>
1	0.09615385	210	0.25696594	30	0	2.78888975	0.03717789	2.78826021
2	0.27272727	210	0.57803762	30	0	3.33042541	0.21694532	3.31078357
3	0.38461538	210	0.68006008	30	0	3.71633724	0.13798082	3.6557749
4	0.5	210	0.77412399	30	0	4.34223209	0.02939583	4.32435298
5	0.6	210	0.84102268	30	0	4.95062556	0.12879599	4.97404468
6	0.63636364	210	0.86850153	30	0	5.3202951	0.07944888	5.31588828
7	0.11111111	100	0.27868852	30	0	2.90371898	0.01335914	2.89591261
8	0.33333333	100	0.56903353	30	0	3.82323419	0.04911873	3.82071601
9	0.5	100	0.74321985	30	0	4.63723745	0.0609458	4.62212834
10	0.6	100	0.81024989	30	0	4.97794787	0.13043189	4.92682871
11	0.66666667	100	0.83388218	30	0	5.11090803	0.0409631	5.11506303
12	0.69230769	100	0.8538961	30	0	4.99847107	0.11237391	4.97341513
13	0.11111111	300	0.21052632	30	0	2.93582584	0.04772857	2.9311672
14	0.33333333	300	0.44880952	30	0	3.83645466	0.02453212	3.84086148
15	0.5	300	0.58854626	30	0	4.40392762	0.08498128	4.42696901
16	0.6	300	0.67280453	30	0	4.5139723	0.08364251	4.55413735
17	0.66666667	300	0.72754313	30	0	4.83743315	0.07864668	4.79462401
18	0.69230769	300	0.74704619	30	0	4.83415951	0.11618446	4.80469675
19	0.5	300	0.56962025	30	2	3.96085299	0.03787127	3.94788434
20	0.11111111	6	0.19	30	0	2.86456121	0.00592911	2.86380575
21	0.33333333	6	0.48813559	30	0	3.13866563	0.00909689	3.1382879
22	0.5	6	0.71965318	30	0	3.75750956	0.04415045	3.77853641
23	0.6	6	0.79161028	30	0	4.27663338	0.04396334	4.30231886
24	0.66666667	6	0.81055156	30	0	4.49785592	0.05567054	4.52454868
25	0.69230769	6	0.84712111	30	0	4.57680101	0.06698384	4.62212834
26	0.11111111	4-Jan	0.22259136	30	0	2.78284611	0.00392142	2.7813352
27	0.33333333	4-Jan	0.54356061	30	0	3.13476244	0.00771804	3.13514017
32	0.11111111	100	0.34146341	30	0	3.19456934	0.0043297	3.19557661
33	0.69230769	100	0.85378835	30	0	4.95717284	0.06010337	4.96271285
34	0.11111111	210	0.3615495	20	0	3.03869369	0.02031884	3.0388196
35	0.33333333	210	0.65570008	20	0	3.9881753	0.00547017	3.98754575
40	0.11111111	210	0.4596577	30	0	3.1614552	0.06255263	3.16346975
41	0.33333333	210	0.65245374	30	0	3.89575791	0.0470781	3.90381611
42	0.5	210	0.78998073	30	0	4.44069312	0.12379623	4.4294872
43	0.6	210	0.83777068	30	0	4.73028438	0.04679312	4.74992622

APPENDIX X – RELATIVE PERMEABILITY OF SAMPLES FABRICATED USING ECOFLEX 30

44	0.66666667	210	0.79794118	30	0	4.95062556	0.03340868	4.94067873
45	0.69230769	210	0.88229084	30	0	5.01420973	0.08724997	5.04392431
47	0.11111111	300	0.1352459	30	1	2.72631286	0.015597	2.72593513
48	0.33333333	300	0.40684932	30	1	3.34843043	0.04561365	3.35359271
49	0.5	300	0.54771784	30	1	4.19126691	0.023095	4.18522327
50	0.6	300	0.68828298	30	1	4.40317217	0.14234944	4.40745308
51	0.66666667	300	0.73511543	30	1	4.75861396	0.12364486	4.76251715
52	0.69230769	300	0.75447427	30	1	4.61633652	0.09632201	4.59946468

APPENDIX XI - BUDGET

BOM (Bill of Materials)	Unit Cost \$	Unit	# of Units	Total \$	Exact or estimated?
Item	\$ 5.00	20 pack	1	\$ 5.00	Exact
Ecoflex 30	\$32	1 pack	2	\$64	Exact
300-micron iron particles (Iron 12)	0 (from lab stock)	1 bottle	1	\$0	Exact
210-micron iron particles (-70 mesh)	0 (from lab stock)	1 bottle	1	\$0	Exact
100-micron iron particles (-20 mesh) (250g)	\$60.80	1 bottle	2	\$121.60	Exact
6-10-micron iron particles (500g)	\$91.40	1 bottle	1	\$91.40	Exact
1-3-micron iron particles (500g)	\$109.00	1 bottle	1	\$109.00	Exact
0.3 mm ID silicon tube (20 ft)	\$34.00	1 pack	1	\$34.00	Exact
0.5 mm ID silicon tube (16 ft)	\$6.89	1 pack	1	\$6.89	Exact
Eutectic Gallium Indium(10g)	\$118.00	1 bottle	1	118	Exact
Silver nano wires (25mL)	\$283	1 bottle	1	283.2	Exact
Bondable wire (26 SAPT EPOXY BOND TYPE 1) (490g)	\$157	1 spool	1	156.8	Exact
Bondable wire (NEMA MW136-C) (504g)	\$151	1 spool	1	151.2	Exact

APPENDIX XI - BUDGET

Please do your best to fill in the following details on your budget	Total \$		Exact or estimated?
Total Development cost: everything that was spent on your project including prototypes, transportation to research locations, renting of equipment, orders from a lab you worked at, your own money etc...?etc...	\$1,136		Estimate
What is the minimum cost to make one prototype of your project (\$0 is an option)?	\$211		Estimate
Total cost of items purchased through the <i>Active Learning Labs (ALL)</i>, if any	\$64		Estimate
Total cost covered by the <i>Harvard Research Lab(s)</i> you are affiliated with, if any	\$1,072		Estimate
Total cost of items purchased personally, if any	0		Exact
Total cost covered by a <i>non-Harvard lab</i> and/or company, if any	0		Exact

Please list below all material used in ALL that were not accounted for in your budget / made available to you at no cost, for e.g.:
22 AWG Wire
28 AWG Wire
30 AWG Wire
1/4 in acrylic plates
25-micron strontium ferrite particles

APPENDIX XII - RLC SERIES CURRENT MATLAB CODE

```

%{
Script for soft EPM Simulations based on equations from
http://www.nessengr.com/technical-data/series-rlc-circuit-equations/
%}

%% Model RLC series current and find peak current

%{
Cases:

Underdamped if  $R^2 < (4L/C)$ 
Overdamped if  $R^2 > (4L/C)$ 
Critically damped if  $R^2 == (4L/C)$ 

%}

% Globally accessible constants
R = 1.413; % Ohms
L = 1.67e-6; % Henries
C = 400e-6; % Farads
t = [0:1e-6:1e-3]; % time from 0 to 1ms
V_o = 30; % Initial voltage on the capacitor (V)

s = (4*L/C); % for checking whether over, under or critically damped

% preallocate global variables
i = zeros(1,length(t)); % current array
w_o = 0; % Oscillation frequency

for j=1:length(t)

    if R^2 < s % Underdamped

        disp('CASE: Underdamped');

        w_o = sqrt( (1/(L*C)) - (R/(2*L))^2 ); % Oscillation frequency

        % Current as at time intervals specified by t
        i(j) = V_o/(w_o * L) * exp((-R*t(j))/(2*L)) * sin (w_o * t(j));

    elseif R^2 > s % Overdamped

        disp('CASE: Overdamped');

        w_o = sqrt((R/(2*L))^2 - (1/(L*C))); % Oscillation frequency

        % Current as at time intervals specified by t
        i(j) = (V_o/(w_o * L)) * exp((-R*t(j))/(2*L)) * sinh (w_o * t(j));
    end
end

```

```

elseif R == s % Critically damped

    disp('CASE: Critically damped');

    % Current as at time intervals specified by t
    i(j) = (V_o * t/L) * exp((-R*t(j))/(2*L));

else
    disp('Error: failed evolutions of damping coefficient')
end

end

%% Extract I_max
[val, idx] = max(i) % max i
t(idx) % value of t at max i

%% Compute peak current

i_peak = 0;
if R^2 == s
    disp('Critically damped')
    % If critically damped
    i_peak = (2*V_o)/(exp(1)*R);

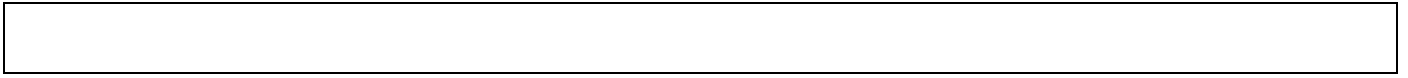
else
    % If underdamped or overdamped
    i_peak = (V_o/(w_o * L)) * exp((-R*pi)/(4*L*w_o));
end

%% Plot Current

figure

% plot and label
plot(t,i);
% line([0,t(end)], [i_peak,i_peak], 'Color','red')
title('Current trough the EP magnet for'...
    + string(' R= ') + string(R) ...
    + string(' L= ') + string(L) ...
    + string(' C= ') + string(C) ...
);
ylabel('current [A]');
xlabel('time [s]');

```



```

%{
Script for sweeping number of turns and diameter of EGaIn tube for a
soft conducive coil. RLC model is based on equations from
http://www.nessengr.com/technical-data/series-rlc-circuit-equations/

%}

% Values of prototype IV (10 turns, 0.3 mm diameter tube, 10mm diameter coil)
%{NOT USED IN THIS PROGRAM but useful for checking correctness of functions}
R = 1.413; % Ohms
L = 1.67e-6; % Henries

C = 400e-6; % Farads
V_o = 30; % Initial voltage on the capacitor (V)

%% Sweep number of turns
close all
clear all

N = [10:1:50];
D = 0.3E-3; %0.3mm Diameter tube
A_tube = (D/2)^2 * pi; % cross sectional area o
C = 400e-6; % Farads
V_o = 30; % Initial voltage on the capacitor (V)

N_out = zeros(1,length(N)); % preallocate
H_N_array = N;
H_out_N = zeros(1,length(H_N_array));
for i=1:length(N)

    max_i = compute_max_current(N(i), A_tube, C, V_o);
    N_out(i) = max_i
    H_out_N(i) = (N(i) * max_i)/7E-3

end

figure
%plot and label
subplot(2,1,1)
plot(N,N_out);
title('Sweeping N with tube diameter=' + string(D) + string('mm')...
    + ' coil length=' + string(7E-3) + string('mm')...
    + ' coil diameter=' + string(10E-3) + string('mm'));
ylabel('Max current [A]');
xlabel('Turns N');

%% Sweep tube sizes

```



```

N = 10;
D = [0.3E-3:0.1E-4:0.5E-3]; %0.3mm Diameter tube
A_tube = (D./2).^2 .* pi; % cross sectional area o
C = 400e-6; % Farads
V_o = 30; % Initial voltage on the capacitor (V)

D_out = zeros(1,length(D)); % preallocate
H_D_array = D;
H_out_D = zeros(1,length(H_D_array));
for i=1:length(D)

    max_i = compute_max_current(N, A_tube(i), C, V_o);
    D_out(i) = max_i
    H_out_D(i) = (N * max_i)/7E-3

end

%plot and label

subplot(2,1,2)

plot(D,D_out);
title('Sweeping D with turns=' + string(N) + string('mm')...
    + ' coil length=' + string(7E-3) + string('mm')...
    + ' coil diameter=' + string(10E-3) + string('mm'));
ylabel('Max current [A]');
xlabel('Diameter D [mm]');

%% Plots for magnetic field strength H

figure
%plot and label
subplot(2,1,1)
plot(H_N_array,H_out_N);
title('Sweeping N to calculate H');
ylabel('Magnetic field strength H [A/m]');
xlabel('Turns N');

subplot(2,1,2)

plot(H_D_array,H_out_D);
title('Sweeping tube D to calculte H')
ylabel('Magnetic field strength,H [A/m]');
xlabel('Diameter D in mm');

%% fuciton to compute max current of coil of 10mm diameter and 7mm length
% params: N - turns, A_tube - tube cross section area, C - capacitance
% V_o - Capacitor charge voltage

function I_max = compute_max_current(N, A_tube, C, V_o)

```

```

%Model RLC series current and find peak current

%{
Cases:

Underdamped if  $R^2 < (4L/C)$ 
Overdamped if  $R^2 > (4L/C)$ 
Critically damped if  $R^2 == (4L/C)$ 

%}

% find inductance of coil
u_0 = 1.257E-6; % permeability of free space m kg s^-2 A^-2
L = (u_0 * N^2 * (pi * (10E-3/2)^2))/7E-3 % L of coil of diameter 10mm and length 7mm

% find resistance of coil
rho_EGaIn = 2.48E-7; % resistivity of EGaIn tube in Ohm meters
R = (rho_EGaIn * N * (pi * 10E-3))/A_tube

t = [0:1e-6:1e-3]; % time from 0 to 1ms

% preallocate global variables
i = zeros(1,length(t)); % current array
w_0 = 0; % Oscillation frequency
s = (4*L/C); % for checking whether over, under or critically damped

for j=1:length(t)

    if  $R^2 < s$  % Underdamped

        %disp('CASE: Underdamped');

        w_o = sqrt( (1/(L*C)) - (R/(2*L))^2 ); % Oscillation frequency

        % Current as at time intervals specified by t
        i(j) = V_o/(w_o * L) * exp((-R*t(j))/(2*L)) * sin (w_o * t(j));

    elseif  $R^2 > s$  % Overdamped

        %disp('CASE: Overdamped');

        w_o = sqrt((R/(2*L))^2 - (1/(L*C))); % Oscillation frequency

        % Current as at time intervals specified by t
        i(j) = (V_o/(w_o * L)) * exp((-R*t(j))/(2*L)) * sinh (w_o * t(j));

    elseif  $R == s$  % Critically damped

        %disp('CASE: Critically damped');

```

APPENDIX XIII - MATLAB CODE FOR ITERATING OVER NUMBER OF TURNS AND DIAMETER OF TUBE

```
% Current as at time intervals specified by t
i(j) = (V_o * t/L) * exp((-R*t(j))/(2*L));

else
    disp('Error: failed evolutions of damping coefficient')
end

end

I_max = max(i);

end
```